

Single-cell RNA sequencing profiles reveal cell type-specific transcriptional regulation networks conditioning fungal invasion in maize roots

Yanyong Cao^{1,2,3,4,†}, Juan Ma^{2,†} , Shengbo Han^{2,5}, Mengwei Hou², Xun Wei³, Xingrui Zhang¹, Zhanyuan J. Zhang^{6,a}, Suli Sun¹, Lixia Ku^{4,5}, Jihua Tang^{4,5}, Zhenying Dong³, Zhendong Zhu¹, Xiaoming Wang¹, Xiaoxiao Zhou², Lili Zhang^{2,5}, Xiangdong Li⁷ , Yan Long^{3,*} , Xiangyuan Wan^{3,*}  and Canxing Duan^{1,*} 

¹Institute of Crop Sciences, Chinese Academy of Agricultural Sciences, Beijing, China

²Institute of Cereal Crops, Henan Academy of Agricultural Sciences, Zhengzhou, China

³Zhongzhi International Institute of Agricultural Biosciences, Research Institute of Biology and Agriculture, University of Science and Technology Beijing, Beijing, China

⁴The Shennong Laboratory, Zhengzhou, China

⁵College of Agronomy, Henan Agricultural University, Zhengzhou, China

⁶Division of Plant Sciences, Plant Transformation Core Facility, University of Missouri, Columbia, Missouri, USA

⁷Department of Plant Pathology, College of Plant Protection, Shandong Agricultural University, Tai'an, China

Received 9 March 2023;

revised 24 April 2023;

accepted 29 May 2023.

*Correspondence (Tel +86 136 9141 2318;

fax 86 10 82109608; email

duancanxing@caas.cn (C.D.), Tel +86 186

0056 1850; fax +86 10 82346928; email

wanxiangyuan@ustb.edu.cn (X.W.) and Tel

+86 158 1133 2686; fax +86 10 82346928;

email longyan@ustb.edu.cn (Y.L.))

^aPresent address: Inari Agriculture, Inc.,

West Lafayette, Indiana 47906, USA

[†]These authors contributed equally to this work.

Keywords: maize stalk rot, scRNA-seq, *Fusarium verticillioides*, co-expression module, immune regulatory networks.

Summary

Stalk rot caused by *Fusarium verticillioides* (*Fv*) is one of the most destructive diseases in maize production. The defence response of root system to *Fv* invasion is important for plant growth and development. Dissection of root cell type-specific response to *Fv* infection and its underlying transcription regulatory networks will aid in understanding the defence mechanism of maize roots to *Fv* invasion. Here, we reported the transcriptomes of 29 217 single cells derived from root tips of two maize inbred lines inoculated with *Fv* and mock condition, and identified seven major cell types with 21 transcriptionally distinct cell clusters. Through the weighted gene co-expression network analysis, we identified 12 *Fv*-responsive regulatory modules from 4049 differentially expressed genes (DEGs) that were activated or repressed by *Fv* infection in these seven cell types. Using a machine-learning approach, we constructed six cell type-specific immune regulatory networks by integrating *Fv*-induced DEGs from the cell type-specific transcriptomes, 16 known maize disease-resistant genes, five experimentally validated genes (*ZmWOX5b*, *ZmPIN1a*, *ZmPAL6*, *ZmCCoAOMT2*, and *ZmCOMT*), and 42 QTL or QTN predicted genes that are associated with *Fv* resistance. Taken together, this study provides not only a global view of maize cell fate determination during root development but also insights into the immune regulatory networks in major cell types of maize root tips at single-cell resolution, thus laying the foundation for dissecting molecular mechanisms underlying disease resistance in maize.

Introduction

Stalk rot is one of the most devastating and prevalent diseases in maize (*Zea mays*) production worldwide, causing yield loss and deterioration of grain quality (Ye *et al.*, 2019), and the disease frequently results from a mixed invasion of two or more causal pathogens (Wang *et al.*, 2017). To establish the disease cycle, *Fusarium* fungi survive from one growing season to the next in soil, infested maize debris or seeds (Gai *et al.*, 2018). They may infect the root system, cause root rot early in the growing season and later grow up into the stalk with the result that stalk rot happens (Gai *et al.*, 2018; Zhang *et al.*, 2016). *Fusarium verticillioides* (*Fv*), an important maize pathogen that produces fumonisin and causes stalk rot and ear rot, has become one of the most aggressive causal agents of maize diseases during recent years (Liu *et al.*, 2019). Previous studies indicate that maize resistance to Gibberella stalk rot caused by *F. graminearum* is a quantitatively inherited trait, and *ZmCCT* and *ZmAUXRP1* have been identified to act in different ways to

confer resistance to *F. graminearum* infection (Wang *et al.*, 2017; Ye *et al.*, 2019). Whereas there is few study on the *Fusarium* stalk rot (FSR) caused by *Fv* in terms of interactions between *Fv* and its host maize plants, and molecular mechanisms underlying maize resistance to *Fv* invasion, which hinders the progress toward effectively controlling the disease in maize molecular breeding.

Roots are not only essential for vascular plant growth and development but also contribute to plant adaptation to challenging environmental conditions. Quantification of gene expression in specific cell types is important for understanding the complex genetic regulatory networks determining root development in responsive to biotic and abiotic stimuli. Single-cell RNA sequencing (scRNA-seq) has been developed to record the diversity of cell types, lineage relationships, and gene expression patterns in plant tissues such as stem, ear, stomata, shoot apex, phloem, and root of *Arabidopsis*, rice, and maize, demonstrating high heterogeneity of these tissues and unprecedented expression signatures of major cell types (Denyer

et al., 2019; Jean-Baptiste et al., 2019; Li et al., 2022; Liu et al., 2020; Marand et al., 2021; Ortiz-Ramírez et al., 2021; Satterlee et al., 2020; Shulse et al., 2019; Xu et al., 2021; Zhang et al., 2019, 2021a,b). Two scRNA-seq specific databases (PCMDB and PlantscRNADB) integrate comprehensive analysis results such as marker genes corresponding to specific cell types in multiple plant species and thus provide useful platforms for annotation of cell types and prediction of biological functions of individual cells (Chen et al., 2021; Jin et al., 2022). scRNA-seq has also been used to investigate responses of different cell types in plant tissues to abiotic stresses (Jean-Baptiste et al., 2019; Li et al., 2022; Shulse et al., 2019). Although single-cell maps of maize roots have been uncovered (Li et al., 2022; Ortiz-Ramírez et al., 2021), the regulatory networks controlling root development in responsive to biotic stimulus such as FSR are still lacking.

Here, by utilizing a single-cell transcriptomic approach to achieve an unbiased sampling of cell types from maize root tips of two inbred lines (Qi319 and B104) inoculated by *Fv* and mock-inoculated with PDA plug as a control, we reported gene expression profiles of maize root tips and specific marker genes for major cell types. By pseudotime analysis, we characterized gene expression changes during root apical meristem (RAM), root cap (RC), stele, and metaxylem development, and found that many specific genes likely direct the differentiation of these root tissues. Then, we identified 4049 differentially expressed genes (DEGs) associated with *Fv* in major cell types, and constructed 12 *Fv*-responsive co-expression modules. Further, we also identified the roles of genes *ZmWOX5b*, *ZmPIN1a*, *ZmPAL6*, *ZmCCoAOMT2*, and *ZmCOMT* in suppressing *Fv* infection in the RAM and other cell types. In addition, many genetic factors and pathways were assigned to six cell type-specific immunity networks, which included the *Fv*-responsive DEGs, potential interactions among genetic factors, maize known resistance genes, and QTL-QTN-predicted genes that are associated with FSR mainly induced by *Fv* and other maize diseases. Collectively, we established a high-resolution cell atlas of maize root tips, constructed six immune regulatory networks controlling *Fv* pathogenesis during maize root development, and demonstrated the significance of scRNA-seq, comparative transcriptome, and integrated bioinformatics by combining QTL mapping and genome-wide association study (GWAS) results to dissect root response mechanisms conditioning fungal invasion.

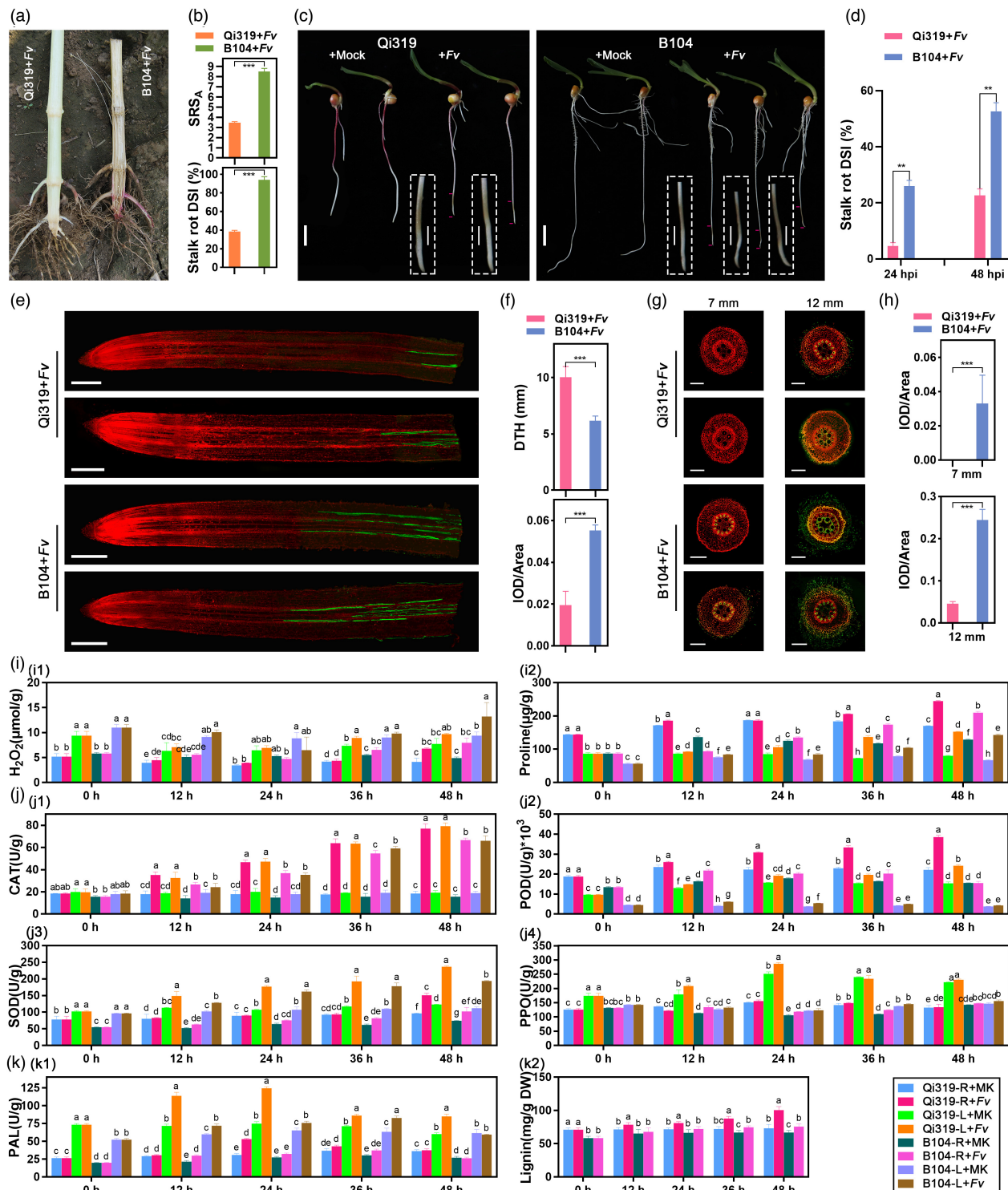
Results

The infection establishment of *Fusarium verticillioides* in maize seedling roots

Compared with inbred line Qi319, one resistant line to maize stalk rot, the susceptible maize inbred line B104 plants displayed more severe rot symptoms in roots and lower stalk interior (Figure 1a), and highly significant increases in the SRS_A (stalk rot score on average) and DSI (disease severity index) after inoculation with *Fv* (Figure 1b). To observe the process of *Fv* proliferation inside maize roots, the primary root tips of both Qi319 and B104 lines were inoculated with *Fv* mycelia plugs and incubated at 26 °C. Both lines displayed different disease severity and speed of lesion progression. For Qi319, light lesions were observed on the diseased region of roots until 36 h postinoculation (hpi), and the diseased roots exhibited generally healthy, with mild and light-brown lesions that were not shrunken symptoms by 48 hpi. In contrast, the light-brown lesions were visible in infected B104 roots as early as 18 hpi, and expanded gradually, reaching approximately 10 mm in length from 36 to 48 hpi, which resulted in approximately 80% of B104 roots developing severe necrotic lesions with dark brown and shrunken in appearance by 48 hpi (Figure 1c, Figure S1a-h). The average DSI of B104 roots was significantly higher with 5.58 and 2.32 times than that of Qi319 roots at 24 and 48 hpi, respectively (Figure 1d).

Although the stalk rot pathogen *Fv* was directly inoculated into the root tips (including RAM), the disease symptoms always appeared above the upper parts of root tips rather than the RAM at different time points postinoculation (Figure 1c, Figure S1a-h). Actually, the diseased part was located in the position of the mycelial inoculum plug at 48 hpi (Figure S1h). As time went by, the lesions spread to the middle part of the inoculated roots. To confirm the observations and assess the connection between the symptom development and colonization of *Fv* in maize roots, the spread of *Fv* hyphae was monitored by WGA-AF488 (wheat-germ agglutinin-Alexa Fluor 488 conjugate) staining. The longitudinal migration of *Fv* was evaluated by measuring the distance between root tip and hyphae (DTH) advancing frontline, and the WGA signals were evaluated by measuring the area density [IOD (integrated optical density) per area] of green fluorescence. For Qi319, *Fv* hyphae were detected mainly in the endodermis and pericycle regions approximately 10–12 mm above the root

Figure 1 The infection establishment of *Fusarium verticillioides* (*Fv*) in maize seedling roots. (a) Images of the longitudinal sections of stalks from resistant (Qi319) and susceptible (B104) maize plants with *Fv* infection. (b) Comparison of stalk rot resistance in Qi319 and B104 maize plants by calculating the stalk rot score on average (SRS_A) and disease severity index (DSI). (c) The rot symptoms of maize seedling roots at 48 hpi with *Fv* infection. Images in the dashed boxes are magnifications of the diseased root regions that are indicated by red arrows. Scale bars = 2 cm (5 mm in dashed boxes). (d) DSI comparison of Qi319 and B104 at 24 and 48 hpi, respectively. (e–h) The spread of *Fv* hyphae was monitored by WGA-AF488 staining at 48 hpi. Staining of the *Fv*-inoculated maize roots with WGA-AF488 results in green-stained *Fv* hyphae, whereas staining of cell walls with propidium iodide (PI) results in red color. Observations were performed by staining the 10–12 mm in length and 5 µm in thick longitudinal slitting slices (e) and transverse sections acquired at approximately 7 and 12 mm from the root tips (g), respectively. The longitudinal migration of *Fv* was evaluated by measuring the distance between the root tip and the hyphae (DTH) advancing frontline (f). The WGA signals of the longitudinal slices (f) and cross sections (h) were evaluated by measuring the area density of the green fluorescence. The area density was indicated as IOD (Integrated Optical Density) per area. Scale bars = 1 mm (e) and 300 µm (g). (i–k) Measurement of physiological and biochemical characters of Qi319 and B104 post *Fv* inoculation. The *Fv* and mock (MK)-inoculated roots (R) and leaves (L) were harvested at 0, 12, 24, 36, and 48 h post-inoculation, respectively. (i) Contents of hydrogen peroxide (H₂O₂) (i1) and ROS scavenger proline (i2); (j) Activities of antioxidant enzymes including catalase (CAT) (j1), peroxidase (POD) (j2), superoxide dismutase (SOD) (j3), and polyphenol oxidase (PPO) (j4); (k) Phenylalanine ammonia-lyase (PAL) activity (k1) and lignin content (k2). Values are mean ± SD. For (b), (d), (f), and (h), *P < 0.05, **P < 0.01, and ***P < 0.001 (paired Student's t-test). For (i–k), different letters on the columns show a significant difference (P < 0.05) as determined by the Tukey–Kramer test.



tips by 48 hpi, and no hypha was observed in the lower portions of the inoculated roots. However, the hyphae spread in a faster and more extensive manner in the inoculated B104 roots than those in Qi319 roots during the same time span (Figure 1e,f). The invasion of *Fv* hyphae was captured at the positions of nearly 6–12 mm from the B104 root tips, in which the spreading regions included stele, endodermis, and epidermis of roots, in the upper

portion of the longitudinal slitting slices, even part of the cortex filled with *Fv* hyphae (Figure 1e,f). These observations were further confirmed by staining the transverse sections acquired at approximately 7 and 12 mm from the root tips, respectively (Figure 1g,h).

Both inbred lines were also characterized by investigating changes in physiological and biochemical parameters of leaves

and roots in responsive to *Fv* invasion (Figure 1*i–k*). In general, higher levels of ROS (reactive oxygen species) including H₂O₂ and MDA (malondialdehyde) were found in B104 seedlings upon *Fv* infection (Figure 1*i1*, Figure S1*i*), while higher activities of antioxidant enzymes such as CAT (catalase), POD (peroxidase), SOD (superoxide dismutase), and PPO (polyphenol oxidase) were observed in Qi319 seedlings (Figure 1*j*). Similarly, the level of ROS scavenger proline in the resistant line Qi319 was more increased upon *Fv* infection (Figure 1*i2*). Additionally, the concentrations of total protein (TP) and water-soluble saccharide (WSS), activities of phenylalanine ammonia-lyase (PAL) and contents of lignin (one of the PAL-related metabolites) displayed more drastic increases in Qi319 seedlings when compared to those in B104 seedlings after exposure to *Fv* (Figure 1*k*, Figure S1*i*).

Collectively, *Fv* only spread above the RAM regions in the inoculated roots of both resistant (Qi319) and susceptible (B104) lines, demonstrating that the RAM, including stem cells and QC, is resistant to *Fv* invasion. Therefore, root tissues approximately 5 mm in length from root tips, which are free of *Fv* invasion and contain RC, RAM, and elongation zone (EZ), were collected at 48 hpi and used to perform subsequent scRNA-seq in this study.

Generation of a maize root tip cell atlas

To perform scRNA-seq of maize roots, maize protoplasts were isolated from root tips of Qi319 and B104 seedlings inoculated with *Fv* at 48 hpi. A total of 38 145 cells were initially mixed with single-cell reaction reagents (Figure S2*a*, Table S1) and the libraries were constructed for 10x Genomics scRNA-seq (Figure 2*a*). Data were filtrated at both cell and gene levels, resulting in a pool of 29 217 cells with 32 224 genes used for further analysis (Table S1). Median genes per cell ranged from 1456 to 2699 in eight samples, and median unique molecular identifiers per cell varied from 2245.5 to 11 005 (Table S1). High correlations (*Spearman r* = 0.94 to 0.97) between two biological replicates of scRNA-seq data indicated the reproducibility in data quality (Figure S2*b*). In addition, the combined scRNA-seq data showed relatively high correlations (*r* = 0.69 to 0.75) with the bulk root mRNA sequencing data (Figure S2*b*), indicating the reliability of scRNA-seq and the effectiveness of maize root protoplast extraction.

After the linear dimensional reduction, the *t*-distributed stochastic neighbourhood embedding (*t*-SNE) tool was used to visualize and explain the scRNA-seq data. An unsupervised analysis grouped maize root cells into 21 clusters (Figure 2*b*). A total of 1950 cell type markers in the 21 clusters were identified and defined after the differential analysis (Table S2). Since only a few experimental results validated marker genes can be used to distinguish maize root cell types, to alleviate this problem, we mined our data to identify potential marker genes that were highly and specifically expressed in one or two clusters (Figure 2*c, d*, Table S2) and also used available information from recent relevant references to select cell type-specific marker genes (Chen et al., 2021; Jin et al., 2022; Ortiz-Ramírez et al., 2021). To validate candidate marker genes *in vivo*, we performed RNA *in situ* hybridization and were able to identify credible cell type-specific markers for distinguishing maize root cell types (Figure 2*e,f*, Figure S3).

For example, *bZIP17*, *TIP1-1*, *Zm00001d003283*, and *Zm00001d017508* were specifically expressed in the cortex cells; *Zm00001d046187* in the endodermis cells; *Zm00001d033711* in the epidermis cells; and *Zm00001d049683*, *UCC3*, and *Zm00001d051333* in the stelle cells. *Cysteine protease5 (CCP5)*

and *Zm00001d032501* were exclusively expressed in the cells of metaxylem (Figure 2*e,f*; Figure S3). *Xylem cysteine peptidase 1 (XCP1)* and *XCP2*, the homology of *CCP5*, are identified as genes encoding xylem-specific cysteine proteases in *Arabidopsis* (Zhao et al., 2000). In addition, *CCP5* is also used as a marker gene for metaxylem in previous studies (Table S3) (Marand et al., 2021; Ortiz-Ramírez et al., 2021). Meanwhile, 38 marker genes were specifically expressed in one or a few clusters, and could be thus used to classify root cell types (Figure 2*d*). For example, the metaxylem marker gene *cellulose synthase13 (CESA13)* was specifically expressed in cluster 19 (Figure 2*d*, Table S3), and also mapped similarly in a previous study (Ortiz-Ramírez et al., 2021).

High accumulations of histone genes *H4C7*, *H4C7.2*, and *his2b1* were demonstrated in cluster 18 (RAM), and high expression of *Zm00001d020794* and *Zm00001d049606* was shown in cluster 13 (RC) (Figure 2*c,e*, Figure S3*b,c*). A series of histone genes are also reported to be involved in RAM development (Kang et al., 2020). In addition, the GO and KEGG functional differences of DEGs between RAM and RC clusters demonstrated their respective cell fates. Specifically, the up-regulated DEGs of cluster 13 relative to cluster 18 were significantly enriched in 17 biological processes (e.g., nucleosome assembly, chromatin organization, glutamine biosynthetic/metabolic process) and three KEGG pathways which were well-known to be involved in RAM development (Figure S2*c*, Table S4) (Garay-Arroyo et al., 2012; Kang et al., 2020; Li et al., 2006; Marquez-Garcia et al., 2014; Shukla et al., 2020). In contrast, the up-regulated DEGs of cluster 18 relative to cluster 13 were significantly involved in 50 GO biological processes and one KEGG pathway that was related to RC development (Figure S2*d*, Table S4) (Tamogami et al., 2021; Thomann et al., 2009; Wei et al., 2009).

Taken together, seven broad populations were revealed using the *t*-SNE projection, and included cortex (clusters 0, 1, 6, 8, 9, 11, 12, 15, and 16), endodermis (clusters 5 and 17), the epidermis (clusters 2, 4, and 7), stelle (clusters 3, 10, 14, and 20), metaxylem (cluster 19), RAM (cluster 18), and RC (cluster 13) (Figure 2*g*). Cortex was the largest population containing 14 305 cells. Stelle, endodermis, and epidermis were the major populations containing cells ranging from 2588 to 6123, whereas a small number of cells (413–758) were observed in RC, metaxylem, and RAM. In each of the homologous cell types, we found that 79%–95% of expressed genes were shared between B104 and Qi319 for the seven cell types upon *Fv* treatment and mock condition (Figure S2*e,f*).

Differentiation trajectories of RAM and RC in maize roots

Developmental state and continuous differentiation trajectory of plant cells can be explored using the scRNA-seq technology. A major difference in the differentiation of plant ground tissue and root cap exists between monocots and dicots, namely, the distal stem cells produce the root cap and the lateral root cap cells lateral to the QC generate the epidermis, and the ground tissue and epidermis belong to a single common initial in monocots, whereas lateral root cap and epidermis share a common initial cell in dicots (Kirschner et al., 2017; Wang et al., 2014). Thus, we attempted to deduce the differentiation trajectories of RAM and RC according to their represented cell clusters using pseudotime analysis. The differentiation trajectories of RAM and RC cells were investigated by pseudotime analysis and the results showed the later differentiation of RC

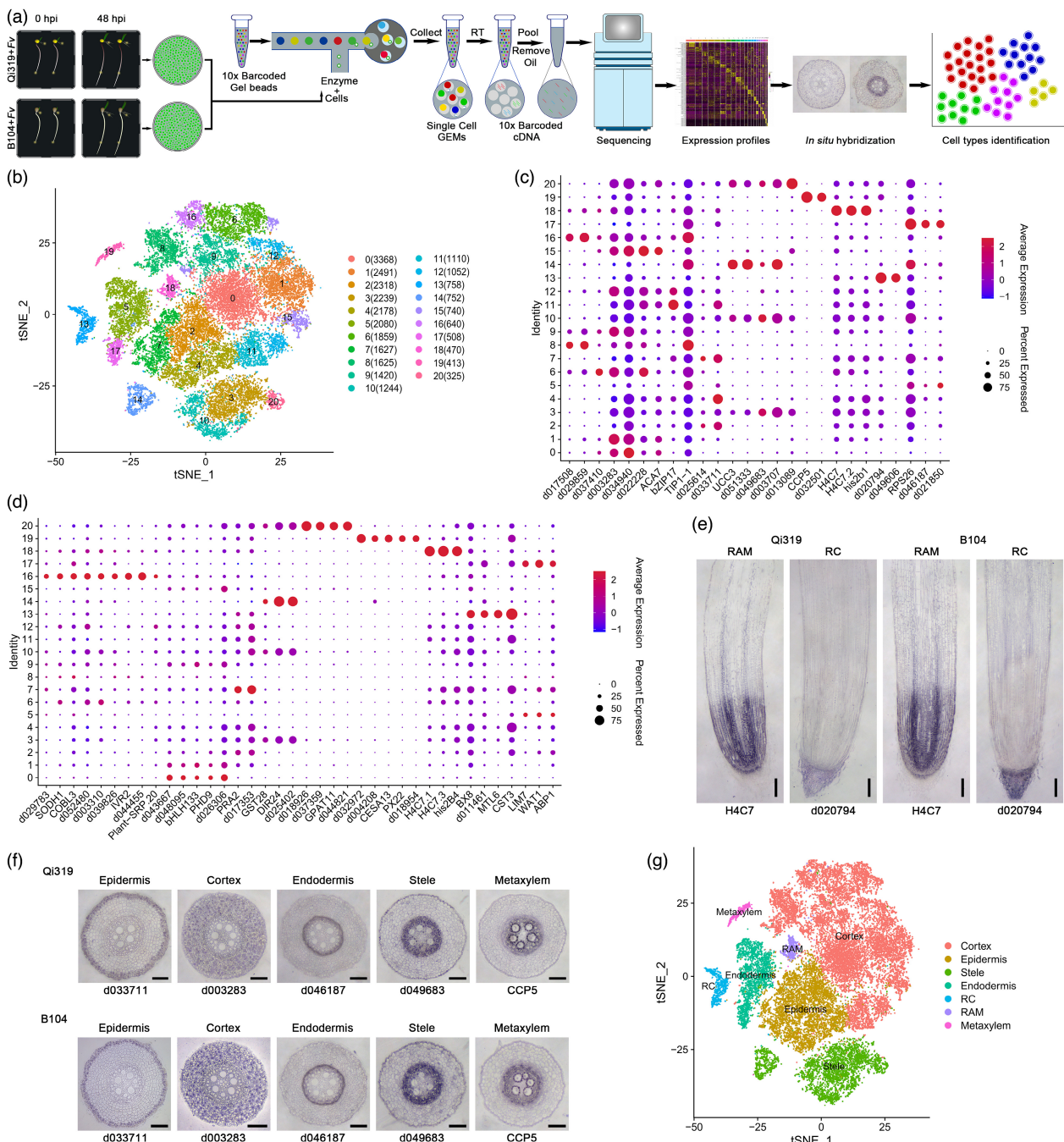


Figure 2 Single-cell RNA-seq and cluster annotation of cell types in maize root tips. (a) Overview scRNA-seq of maize root tips and cell type cluster annotation flowchart. Protoplasts were isolated from 5-mm root tips of maize Qi319 and B104 seedlings at 48 h post-Fv-inoculation or mock-infestation, respectively. The scRNA-seq libraries were generated using the 10x Genomics platform followed by high-throughput sequencing. (b) Visualization of 21 cell clusters in maize root tips using t-SNE. Each dot represents a single cell. Colors represent different cell clusters. (c) Expression patterns of 26 cell cluster-specific marker genes validated using *in situ* hybridization. Dot diameter represents the proportion of a given gene expressing in one specific cell cluster, and color represents their relative expression levels in these cell clusters. (d) Expression patterns of 38 representative cell cluster-specific marker genes in the 21 cell clusters. (e–f) RNA *in situ* hybridization validation of representative cell type-specific marker genes for the putative RAM (root apical meristem) and RC (root cap) regions (e), and epidermis, cortex, endodermis, stele, and metaxylem (f) in Qi319 and B104 roots, respectively. Scale bars = 200 µm in (e) and 150 µm in (f). (g) Visualization of seven broad populations and their spatial distribution in maize root tips using t-SNE.

compared to that of RAM (Figure 3a,b). These results support the accuracy of scRNA-seq and cell classification in maize roots in this study.

To identify key genes controlling the transition of differentiation between RAM and RC cells, we performed branched expression analysis modelling, which uses penalized splines to infer the

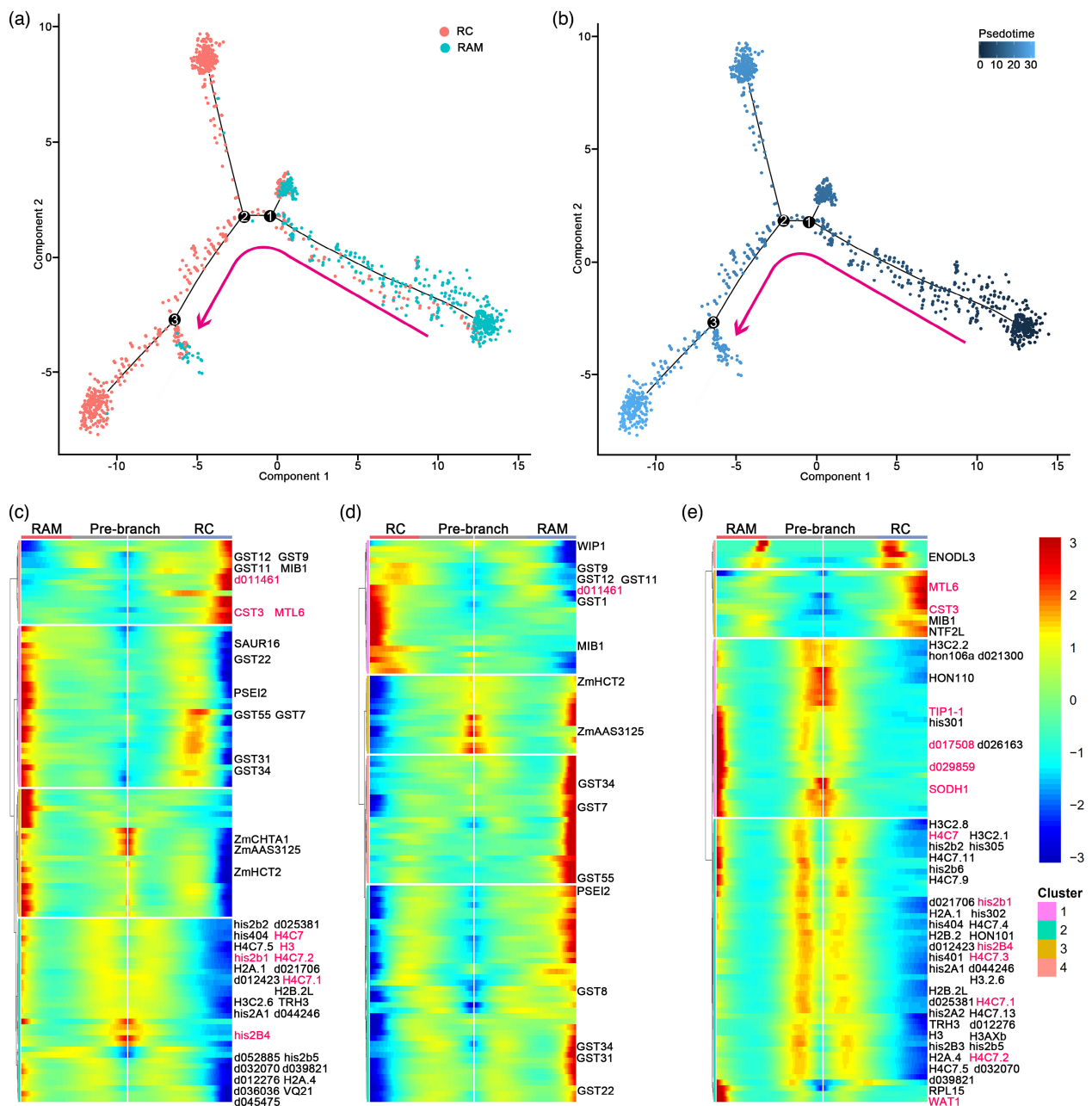


Figure 3 Differentiation trajectories between root apical meristem and root cap in maize roots. (a) Colored pseudotime trajectory of root apical meristem (RAM) and root cap (RC). (b) Distribution of cells on the pseudotime trajectory of RAM and RC. (c–e) Heatmap showing the top 100 significantly changed genes in three branch points during the differentiation trajectory between RAM and RC.

individual gene branching time. The differentiation trajectories between RAM and RC had three branch points marked as 1, 2, and 3 (Figure 3c–e). We investigated the top 100 significantly changed genes for each branch point and displayed its representative genes. For each branch point, these genes all fell into four clusters with distinct gene expression patterns that manifested transcriptional rewiring during root development (Figure 3c–e). The expression patterns of marker genes differed greatly especially at branch point 3 during RC and RAM differentiation (Figure 3e). During the differentiation trajectory between RAM and RC, 24 and 43 histone family members were significantly altered at branch point 1 and 3, and none was found at branch point 2 (Figure 3c,e). Eight and 11 genes encoding glutathione transferase were only observed at

branch point 1 and 2, respectively (Figure 3c,d), indicating their key roles in RAM and RC cell differentiation. These findings provide insights into the dynamic differentiation of root cell development and the rewiring of crucial gene expression during the transition of cell states in maize roots.

Fv-responsive genes vary in maize genotypes and root cell types

To identify *Fv*-responsive genes, the differential expression analysis was performed in seven cell populations between *Fv* treatment and mock condition in two genotypes (Qi319 and B104). A total of 4049 genes showed significant expression in root cell types of both genotypes. The total number of

Fv-induced DEGs was higher in Qi319 than that in B104 across the seven cell types except stele. Upon challenge with *Fv*, the number of up-regulated DEGs (254–578) was consistently lower than that of down-regulated DEGs (346–972) in all the seven cell types of Qi319. In contrast, B104 recruited more up-regulated DEGs in response to *Fv* invasion in all the seven cell types (Figure S4a).

Fv-responsive genes 67.69%–93.67% were overlapped in at least two cell types of B104 and Qi319 (Figure S4b,c), suggesting that different types of root cells can recruit the same sets of genes in responsive to *Fv* infection. Among them, six conserved genes including *maize insect resistance3 (MIR3)*, *benzoxazinone synthesis11 (BX11)*, *shrunken1 (Sh1)*, *subtilisin-chymotrypsin inhibitor homolog1 (SCI1)*, *Zm00001d034382*, and *Zm00001d031677* were differentially expressed upon *Fv* infection across all the seven cell types in Qi319 and B104 (Figure S4d). Notably, these six DEGs were all up-regulated upon *Fv* invasion across all the seven cell types of susceptible line B104 but almost repressed in resistant line Qi319 (Figure S4e). In the same cell type, most of the *Fv*-responsive DEGs were specific to B104 or Qi319, with the proportions of specific DEGs from 67.5% to 91.80% and from 57.91% to 78.42% in Qi319 and B104, respectively (Figure S4f).

Most of the marker genes showed significant expression variations in their corresponding cell types of two genotypes upon *Fv* infection (Figure S5a,b). For example, *bZIP17* was up-regulated in cortex cells of both genotypes. *CCP5* showed significant expression differences in metaxylem cells of B104. *H4C7.2* and *his2b1* were highly activated in RAM cells of Qi319 but repressed in B104. Notably, we also found 32 known plant disease-related genes were significantly differentially expressed in B104 and Qi319 lines (Figure S5c, Table S5). Most of these genes showed significantly differential expression upon *Fv* infection in all the seven cell types of Qi319, whereas a few of them were found in B104 (Figure S5c). Among them, *ZmPAL1* was highly induced after *Fv* infection in all seven cell types of B104 but significantly repressed in the seven cell types except metaxylem of Qi319. *ZmCAT1*, *ZmLOX3*, and *ZmLOX4* were down-regulated across almost seven cell types of Qi319. In particular, the differential expression profiles of these four genes in response to *Fv* invasion in the seven cell types were largely consistent with those in bulk RNA-seq (Figure S5c) and real-time RT-PCR validation (Figure S6b,c).

To determine whether the *Fv*-responsive DEGs are involved in disease-related pathways, we conducted the GO and KEGG analyses. In all seven cell types, 60%–77.42% of GO terms were associated with biological processes such as phenylpropanoid, lignin, and flavonoid biosynthetic processes, defence response to fungus, and pathogenesis (Figure S5d, Table S6), which are involved in protecting roots against pathogens (Lee *et al.*, 2019; Treutter, 2006; Yadav *et al.*, 2020). KEGG analysis also showed that *Fv*-induced DEGs were significantly enriched in phenylalanine, phenylpropanoid, and flavonoid biosynthetic pathways, and plant-pathogen interaction (Figure S5e). Collectively, these findings indicate that major cell types of maize roots play important roles in responsive to *Fv* invasion through multiple disease-related pathways.

Co-expression regulatory modules with key gene regulators in seven root cell types in responsive to *Fv* infection

To define clusters of co-expression genes, a gene co-expression network analysis of 4049 DEGs in all seven cell types was

performed using the WGCNA package. The resultant co-expression network was composed of 15 modules (M1 to M15) harbouring 67 to 1297 genes and one unassigned module (M16) (Figure 4a, Table S7). Fourteen modules (M1–7 and M9–15) were significantly correlated with the seven cell types of B104 and Qi319 upon *Fv* invasion and mock, with *r* values ranging from 0.41 to 0.85. Among them, eight (M1–4, 6, 7, 12, and 15) and 12 (M1, 2, 4–7, and 9–14) (Figure 4b) modules were significantly associated with mock and *Fv* treatment, respectively (Table S7). Most of these significant modules were specific to one cell type. For example, M3 and M15 were specifically correlated with endodermis cells in B104 roots and cortex cells in Qi319 roots under mock condition, respectively. Upon *Fv* invasion, M11, M13, and M14 modules were specifically correlated with metaxylem, epidermis, and cortex cells in Qi319 roots, respectively. Seven modules (M1, 2, 4, 6, 7, 9, and 12) were significantly associated with two or three samples that represented different cell types, genotypes, or treatments (Table S7).

We also found that most of the marker genes shown in Figure 2c,d were clustered into their corresponding cell types using the WGCNA (Figure 4b). In particular, five histone genes *H4C7*, *H4C7.2*, *H4C7.3*, *his2b1*, and *his2B4* were found in M6 module which represented RAM. In this module, 48 DEGs were histone genes, accounting for 58.54% of all DEGs, highlighting the roles of histone family in the development of RAM (Table S7). This finding suggests that the co-expression network analysis can be used for the classification of cell types according to the expression patterns of marker genes in certain cell types.

In *Fv*-responsive modules, 41 marker genes and 19 reported resistant genes were found (Table S7). Moreover, through integrating published QTLs and QTNs that were associated with maize Fusarium ear rot (FER) disease and other 24 diseases (pathogens), we found that 86 genes out of 195 overlapped genes among 4049 *Fv*-induced DEGs, previously published 85 QTL clusters, and 358 QTN clusters (Figure S5f, Table S8) were involved in *Fv*-responsive co-expression modules. Two resistant genes (*ZmCHTA1* and *ZmHCT2*) and 12 QTL/QTN predicted genes were significantly differentially expressed at different branch points in maize root cell differentiation and development (Figure 3e–j, Table S6). Therefore, these genes might be key genetic factors in response to *Fv* infection at single-cell resolution.

Elucidating gene regulatory networks (GRNs) is crucial to understand plant protection mechanisms in response to disease infection. A machine-learning method GENIE3 was used to predict target genes of 148 key regulators including 19 reported resistant genes (ABP1 also a marker gene), 86 QTL/QTN predicted genes, 41 marker genes (including ABP1), *ZmWOX5b*, *ZmPIN1a*, and *ZmYUC6* in each significant *Fv*-responsive module (Table S9). Many regulatory genes and their complex GRNs were especially observed in M11 and M12 which both correspond to metaxylem cells (Table S9). We demonstrated their GRNs using Cytoscape in Figure 4b.

In particular, *uaz248a (his3)*, a QTL/QTN predicted *Fv*-responsive gene (Table S7), potentially interacted with three marker genes (*H4C7*, *his2b1*, and *H4C7.2*), *ZmPIN1a*, and *ZmWOX5b* in module M6 of RAM cells (Figure 4b, Table S9). A previous study showed that *WOX11* (the homology of *ZmWOX5b*) recruits a histone H3K27me3 demethylase to promote gene expression during shoot development in rice (Cheng *et al.*, 2018). The spatio-temporal expression of *PIN* genes, at least for *PIN1*, is fine-tuned by both H3K27 methylation and demethylation, which coordinates to ensure proper lateral

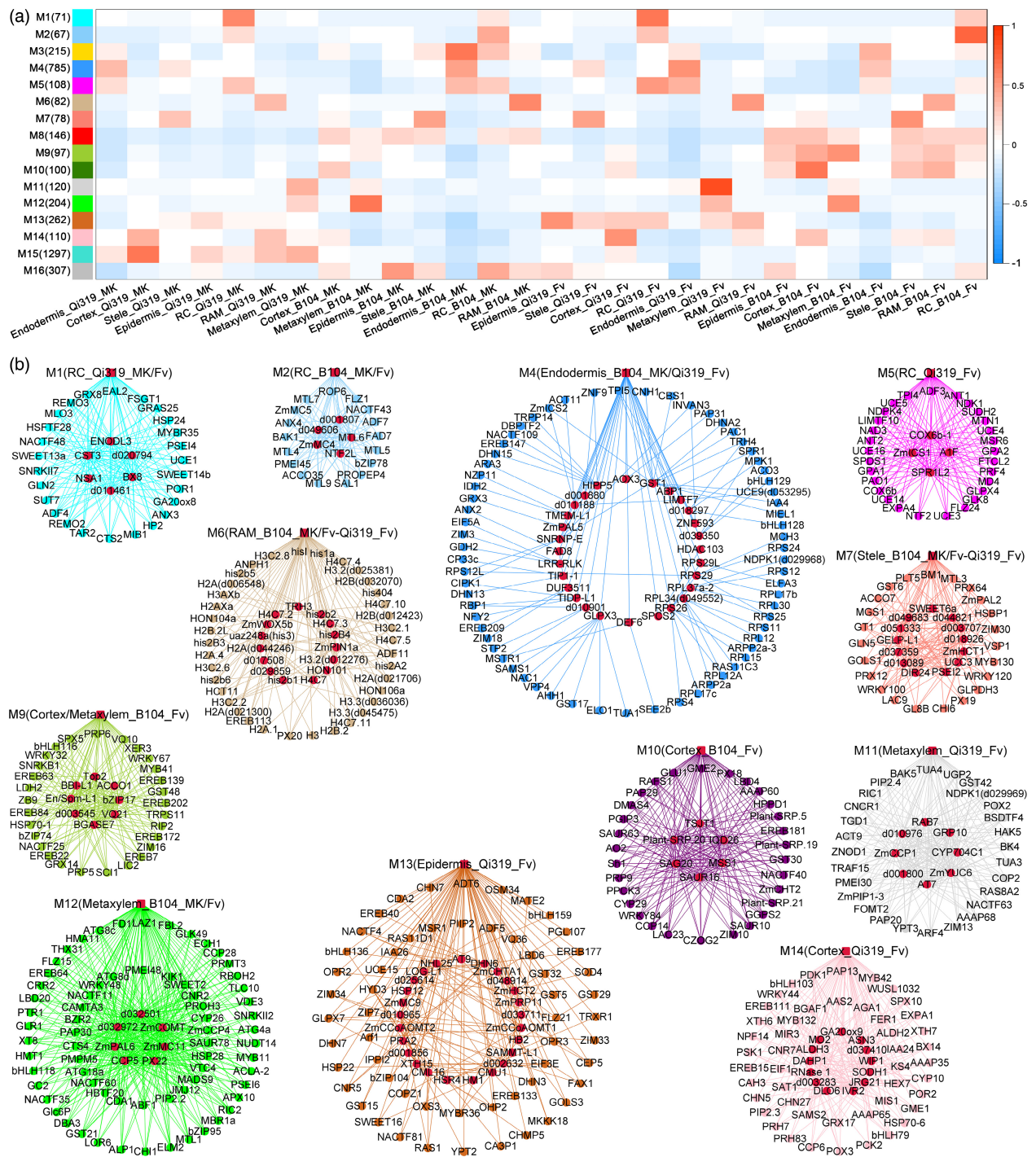


Figure 4 Co-expression regulatory modules with key gene regulators in seven root cell types in responsive to *Fv* infection. (a) 16 co-expression modules associated with each cell type of B104 and Qi319 root tips post *Fv* infection and mock inoculation. The number in the bracket denotes the number of genes in each module. Red and blue represent high and low correlation coefficient values (Pearson), respectively. M16 denotes an unassigned module. MK, mock; RAM, root apical meristem; RC, root cap. (b) 12 gene regulatory modules harboring key gene regulators in responsive to *Fv* infection by GENIE3. Each node represents a gene, and genes exhibiting a regulatory relationship are connected with edges. Red color represents *Fv*-responsive regulatory modules and key regulators, and other colors represent the predicted target genes regulated by these key regulators. The target genes with annotations are shown using Cytoscape (Table S9). The predicted target genes of five regulatory genes (*ZmFNS1*, *ZmAPX2*, *INCW1*, *TUB6*, and *Zm00001d048667*) in Table S7 are not found. The gene regulatory networks of *WAT1*, *Zm00001d032517*, *Zm00001d016664*, *Zm00001d048908*, and *Zm00001d001862* in Table S9 are not shown.

root organogenesis (Wang et al., 2019). These results indicate the significance of GRN analysis for identification of putative disease resistance genes and their regulatory networks.

ZmWOX5b and ZmPIN1a suppress *Fv* invasion in maize RAM via regulating IAA signalling

Plant stem cells and their constantly differentiated daughter cells in apical meristem are expected to safeguard the integrity of cells from biological invasion (Wu et al., 2020). The characteristics of RAM free of *Fv* infection observed in this study promote us to explore its underlying molecular mechanism. *ZmWOX5b* and *ZmPIN1a* were found to be up-regulated in RAM cells upon *Fv* invasion and were thus speculated to be key genes of the *Fv*-responsive regulatory module M6 (Figure 4b, Figure S6a). To test whether *ZmWOX5b* and *ZmPIN1a* are involved in the host defence against *Fv* invasion in maize RAM, transgenic maize plants enhancing expression of *ZmWOX5b* and *ZmPIN1a* were generated by fusing both the native genes and 35S promoters (Figure S7a,b) and transforming into inbred line B104, respectively. Homozygous lines WE8-6 and WE12-2 (enhancing expression of *ZmWOX5b*), and PE6-2 and PE10-4 (enhancing expression of *ZmPIN1a*) were obtained and propagated to T₄ generations (Figure S7c,d), which were used for subsequent analysis. These four over-expressing lines (shown as WE⁺ and PE⁺) displayed 26- to 33-fold enhanced expression of *ZmWOX5b* and *ZmPIN1a* relative to their non-transgenic siblings (WE⁻ and PE⁻) (Figure S7e,f). This result was confirmed by the RNA *in situ* hybridization and GFP observations (Figure 5a,b). Furthermore, transgenic maize events (shown as WR⁺ and PR⁺) were obtained by using RNA interference (RNAi)-mediated silencing of *ZmWOX5b* and *ZmPIN1a* (Figure S7g,h), among which, four representative homozygous lines WR2-6, WR3-4, PR6-1, and PR7-4 (Figure S7i,j) displayed the significantly reduced expression of *ZmWOX5b* and *ZmPIN1a* (Figure S7k,l).

The enhanced expression lines of *ZmWOX5b* and *ZmPIN1a* developed deeper roots, with longer primary and seminal roots than the non-transgenic lines post fungal infection (Figure 5c,d1, d3). In contrast, the primary and seminal root growth was significantly arrested in the four RNAi lines compared to that in the transgene-negative siblings (Figure 5c,d2,d4). Meanwhile, over-expression of *ZmWOX5b* and *ZmPIN1a* significantly retarded the development of root rot symptoms in primary roots upon *Fv* invasion. At 48 hpi of *Fv* infection, seedling roots of the four over-expressing lines generally displayed mild rot symptoms such as light-brown colour lesions, while those of the non-transgenic lines exhibited severe rot symptoms such as dark-brown lesions and shrunk roots. In contrast, the RNAi-positive transgenic plants displayed even more severe rot symptoms compared to their transgene-negative siblings (Figure 5c). Accordingly, the four over-expressing transgenic seedlings displayed drastically lower DSI values than their non-transgenic siblings, while the four RNAi lines showed significantly higher DSI values than their transgene-negative siblings (Figure 5e1,e2). Accordingly, over expression of *ZmWOX5b* and *ZmPIN1a* resulted in a significant induction of maize disease resistance-related marker genes after fungal inoculation, respectively (Figure S8).

In addition, we investigated the *Fv* colonization in maize roots using the WGA staining and found that only a few of *Fv* hyphae were visible in the vascular tissue of the upper parts in the over-expression transgenic roots at 24 hpi, but massive *Fv* hyphae colonized in almost the entire vascular tissue and spread as far as the marginal zone of the RAM in the RNAi transgenic lines (Figure 5f). These observations were further confirmed by the

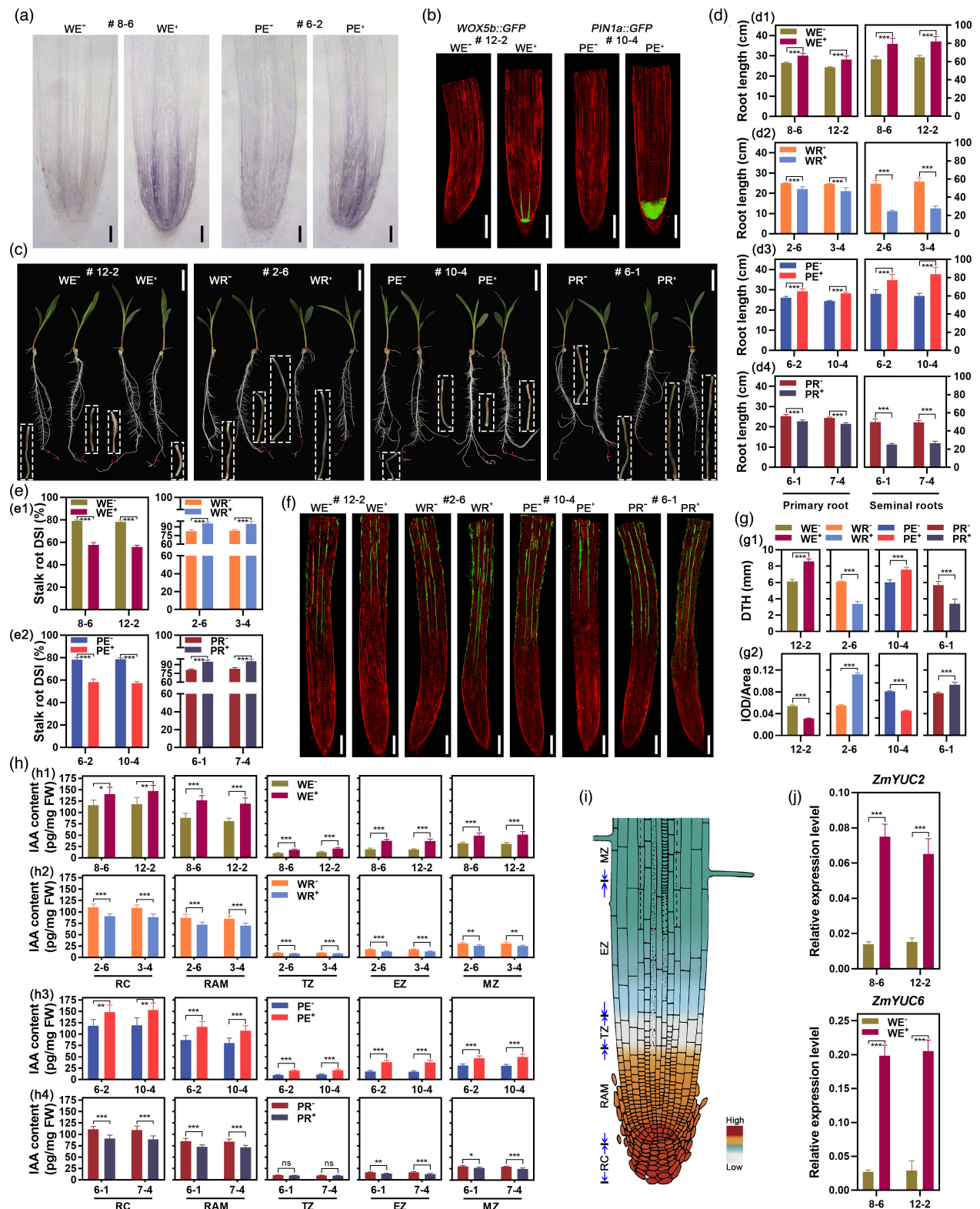
measurement of DTH and IOD per area (Figure 5g). These results indicate that *ZmWOX5b* and *ZmPIN1a* are involved in innate anti-fungal invasion in maize RAM.

To explore the potential mechanisms of *ZmWOX5b* and *ZmPIN1a* in protecting maize root from *Fv* invasion, we collected the different segments of maize root tips including RC, RAM, transition zone (TZ), EZ, and maturation zone (MZ) and then measured their 3-Indole acetic acid (IAA) contents. As a result, the IAA levels exhibited significantly higher throughout the five regions in root tips of the *ZmWOX5b* and *ZmPIN1a* over-expressing lines (Figure 5h1,h3), while significantly lower in the RNAi positive lines (Figure 5h2,h4) when compared to their controls. Notably, the IAA concentration gradients in the root tips were observed based on the IAA contents among different regions (Figure 5h,i). In addition, several previous studies have reported that *WOX* genes are involved in auxin signalling in shoot and root stem cell maintenance (Ma et al., 2019; Tian et al., 2014). To test whether *ZmWOX5b* influences auxin biosynthesis, transcript levels of five IAA biosynthesis-related *ZmYUC* genes (*ZmYUC2*, 4, 5, 6, and 9) (Suzuki et al., 2016) were determined by using 15-mm regions of the primary root tips in the *ZmWOX5b* over-expressing lines. Among them, the expression of *ZmYUC2* and *ZmYUC6* was significantly stimulated by the enhanced expression of *ZmWOX5b* in root tip segments (Figure 5j). Collectively, these results demonstrate that *ZmWOX5b* and *ZmPIN1a* can suppress *Fv* infection in the RAM through regulating IAA biosynthesis, which results in forming IAA concentration gradient and protects the RAM from *Fv* infection to facilitate root elongation in maize.

Phenylpropanoid pathway-related genes participate in *Fv* defence in several types of root cells

Differential expression of phenylpropanoid-related genes in root cells especially in the cortex, stele, and vascular cells postinoculation (Figures S5c and S6) urged us to explore whether these genes are involved in coordinating host defences in response to microbial attack. Among them, *ZmPAL6* (in M4), *ZmCOMT* (in M12), and *ZmCCoAOMT2* (in M13) that present in different GRNs upon *Fv* invasion (Figure 4b), were selected for virus-induced gene silencing (VIGS) to test their potential roles in anti-fungal invasion (Table S10). The silencing efficiency measurement indicated that transcript levels of *ZmPAL6*, *ZmCOMT*, and *ZmCCoAOMT2* were reduced by 80%-85% in their silenced maize plants compared with the control plants (Figure 6a-c). In the *ZmCCoAOMT2*-silenced plants, expression of *ZmCCoAOMT1*, which exhibits 83% identity with *ZmCCoAOMT2* (Guillaumie et al., 2007) was not affected (Figure 6b2). Similarly, in the *ZmPAL6*-silenced plants, the expression of *ZmPAL1*, 3, and 5 was not affected (Figure 6a2-a4). Thus, gene silencing lines of these three genes had been successfully achieved for subsequent analysis.

At 7 dpi, the BMV-GFP- and chimeric-BMVCP5-pre-inoculated maize Va35 plants were challenged with *Fv* invasion, respectively. By measuring the rot symptoms and DSI of these plants, we found that the silencing of *ZmPAL6*, *ZmCOMT*, and *ZmCCoAOMT2* facilitated the *Fv* infection in the silenced-plant roots, and caused more severe rot symptoms than those in the control roots (Figure 6d). Moreover, the DSI was in consistent with the development of rot symptoms, namely, the silencing of these three genes in maize plant roots through VIGS caused approximately by 25%-35% increase of DSI compared to those in the control roots (Figure 6e). In addition, increasing evidence indicates that the phenylpropanoid pathway providing the



lignin-building monolignols can be greatly triggered after the cell wall gets hit by pathogens (Yadav *et al.*, 2020). We thus investigated whether *Fv* infection increases lignin biosynthesis, and found that *ZmPAL6*-, *ZmCOMT1*-, and *ZmCCoAOMT2*-silenced maize plant roots accumulated less lignin than the control roots when infected by *Fv* (Figure 6f). To further explore

the distribution of lignin deposition in these plant roots, transverse ultrathin sections were prepared from the lower-root segments immediately adjacent to the lesions, which lacked visible rot symptoms and were used for Maule staining. Cell wall lignification or thickening was observed in the hypodermal cells of the control roots rather than in the silenced roots. Moreover,

Figure 5 *ZmWOX5b* and *ZmPIN1a* suppress *Fv* invasion in maize RAM via regulating IAA signaling. (a) Transcriptional levels of *ZmWOX5b* and *ZmPIN1a* in the RAM of root tips in the enhanced expression transgenic events (WE⁺ 8-6 and PE⁺ 6-2) and their non-transgenic ones by RNA *in situ* hybridization. Scale bars = 205 µm. (b) GFP fluorescence of transgenic seedling roots transformed with *ZmWOX5b::GFP* and *ZmPIN1a::GFP* fusion constructs shows their expression in the RAM. Scale bars = 500 µm. (c) The rot symptoms of *ZmWOX5b*- and *ZmPIN1a*-transgenic seedling roots (WE⁺ and PE⁺ for enhanced expression; WR⁺ and PR⁺ for RNAi) at 48 hpi with *Fv* infection. Images in the dashed boxes are magnifications of the diseased root regions that are indicated by red arrows. Scale bars = 4 cm. (d) Length comparison of primary and seminal roots in *ZmWOX5b*- and *ZmPIN1a*-enhanced expression (d1 and d3) and RNAi (d2 and d4) transgenic maize seedlings at 48 hpi. (e) DSI of the *ZmWOX5b*- (e1) and *ZmPIN1a*- (e2) transgenic seedling roots was evaluated and compared at 48 hpi, which was significantly decreased in the WE⁺ and PE⁺ plants compared to that in the WR⁺ and PR⁺ plants and the transgene-negative ones (WE⁻, PE⁻, WR⁻, and PR⁻). (f) *Fv* fungal colonization in the root tips of transgenic seedlings was monitored by WGA-AF488 staining at 24 hpi. Scale bars = 500 µm. (g) Measurements of *Fv* hyphal advance distances in the *ZmWOX5b*- and *ZmPIN1a*-transgenic seedling roots by measuring the distance between the root tip and the hyphae (DTH) advancing frontline (g1) based on images of longitudinal slices as illustrated in (f). The WGA signals of the longitudinal slices were evaluated by calculating the area density (i.e., IOD) of green fluorescence to shed light on the process of *Fv* proliferation inside root tips (g2). (h) The enhanced expression of *ZmWOX5b* and *ZmPIN1a* increased the IAA content and auxin concentration gradients in maize root tips. Different segments of root tips including RC, RAM, TZ (transition zone), EZ (elongation zone), and MZ (maturation zone) were sampled and used to measure the IAA contents in the *ZmWOX5b*-overexpression (h1) and -RNAi (h2) lines, and *ZmPIN1a*-overexpression (h3) and -RNAi (h4) lines by GC-MS. (i) The cartoon provides a schematic representation of a maize root tip indicating the different segments and IAA concentration gradients. (j) Transcriptional levels of auxin biosynthetic pathway-related *YUC* genes in the 5–10 mm region (*ZmYUC2*) (j1) and 0–5 mm section (*ZmYUC6*) (j2) of root tips collected from *ZmWOX5b* enhance-expression seedlings. For (d), (e), (g), (h), and (j), values are mean ± SD. *P < 0.05, **P < 0.01, and ***P < 0.001 (according to a paired Student's t-test).

high levels of lignin were deposited in exodermal and vascular cylinder in the control roots, whereas weak lignin staining was observed within the vascular tissues of the silenced roots (Figure 6g). These results suggest that phenols involved in lignin biosynthesis might slow or suppress *Fv* propagation.

Many PALs have been shown to confer broad-spectrum antimicrobial activities and also contribute to the host defence against microbial infection (Ning and Wang, 2018; Yadav *et al.*, 2020). To investigate whether *ZmPAL6* modulates host responses to multiple pathogens, we examined its silencing effect on the infection of *F. proliferatum* (*Fp*) and *Pythium aristosporum* (*Pa*), which also are the predominant causal agents of maize stalk rot (Duan *et al.*, 2022; Liu *et al.*, 2019). The silencing of *ZmPAL6* significantly promoted the infection of *Fp* and *Pa* in maize roots by measuring DSI (Figure 6h). In addition, PAL is the key enzyme in the biosynthetic pathway of salicylic acid (SA) (Zhang and Li, 2019). We found that the SA content was increased by *Fv* infection, however, its accumulation in *ZmPAL6*-silenced plant roots was not as intensively increased in BMV-GFP infected plant roots (Figure 6i). Consistently, knockdown of *ZmPAL6* impaired expression of SA-responsive genes *ZmPR3*, 4, 5, and 10 (Figure 6j). Thus, SA can be synthesized through PAL-dependent route and the *Fv*-induced SA accumulation may attribute to activating the phenylpropanoid pathway.

Construction of cell type-specific immune regulatory networks in maize roots

After Figure 4 demonstrates what extent *Fv*-infection induces gene co-expression modules in different root cell types, considering the diverse functions of root cell types in biotic stress responses (Rich-Griffin *et al.*, 2020), the integrated immunity regulatory networks based on cell type-specific immunity modules are critical for deep understanding of molecular mechanisms underlying maize root defence to fungal invasion. Among the genes that appeared in the GRNs, 16 known disease-related genes and 42 QTL/QTN predicted genes that associated with FER (mainly caused by *Fv*) (Figure 4b, Table S10) were selected to construct the integrated immunity regulatory networks, in which the root cell types and the specific gene co-expression modules were labelled with different colours

(Figure 7a). The integrated regulatory networks consisted of four main elements, namely, the known and predicted disease-related genes and their cell types with the top three expression abundance among seven root cell types, disease-resistance signalling or metabolic pathways, and regulatory connections predicted by the machine-learning method GENIE3 (Figure 7b–g; Table S10).

RC and epidermis as outer and environment-facing cell layers, are important in protecting roots against pathogen invasion. For three RC- or epidermis-specific gene co-expression modules including the M1, M2, and M13 (Figure 4b), phenylpropanoid pathway-related genes such as *ZmCCoAOMT1/2* and *ZmHCT1/2* act as key components to wave this immune network by connecting other genes in RC and epidermis cells of maize roots. These genes in this network are associated with defence hormones (e.g., SA, JA, ET, CK, and ABA) signalling, ROS producing and scavenging, hypersensitive response (HR), PCD, biosynthesis of secondary metabolites (e.g., lignin, phytoalexins, flavonoids, and cell wall), developmental processes, etc (Figure 7b).

Cortex is also the outer layer of root, lying below the epidermis but outside of the vascular bundles, and involved in root immune response to fungal infection (Kawa and Brady, 2022). In the M14 module (Figure 4b), biosynthesis of flavonoids via the shikimate pathway might serve as a key element that connects transcription factors (TFs, e.g., MBY42 and bHLH103) to activate this cortex-specific immune network, and genes in this network are enriched and associated with ROS metabolism, defensive metabolites (lignin and coumarins) biosynthesis, and defence hormones (e.g., JA and SA) signalling (Figure 7c). In addition, the M9 module (Figure 4b) represents two cell types, and its associated genes participate in the induction of ETI (effector-triggered immunity) and the downstream defensive responses through hormones (e.g., JA and SA) signalling, ROS burst, and PCD (Figure 7d). Genes in the stele-specific M7 module (Figure 4b) are associated with defence hormones signalling, lipid metabolism, and sugar transport (Figure 7e).

The interplay between the RAM-specific M6 and metaxylem-specific M11 and M12 modules provides novel regulatory mechanisms at the gene expression level to support this crosstalk between the IAA- and SA-related defence pathways (Figures 5 and 7f). SA is a

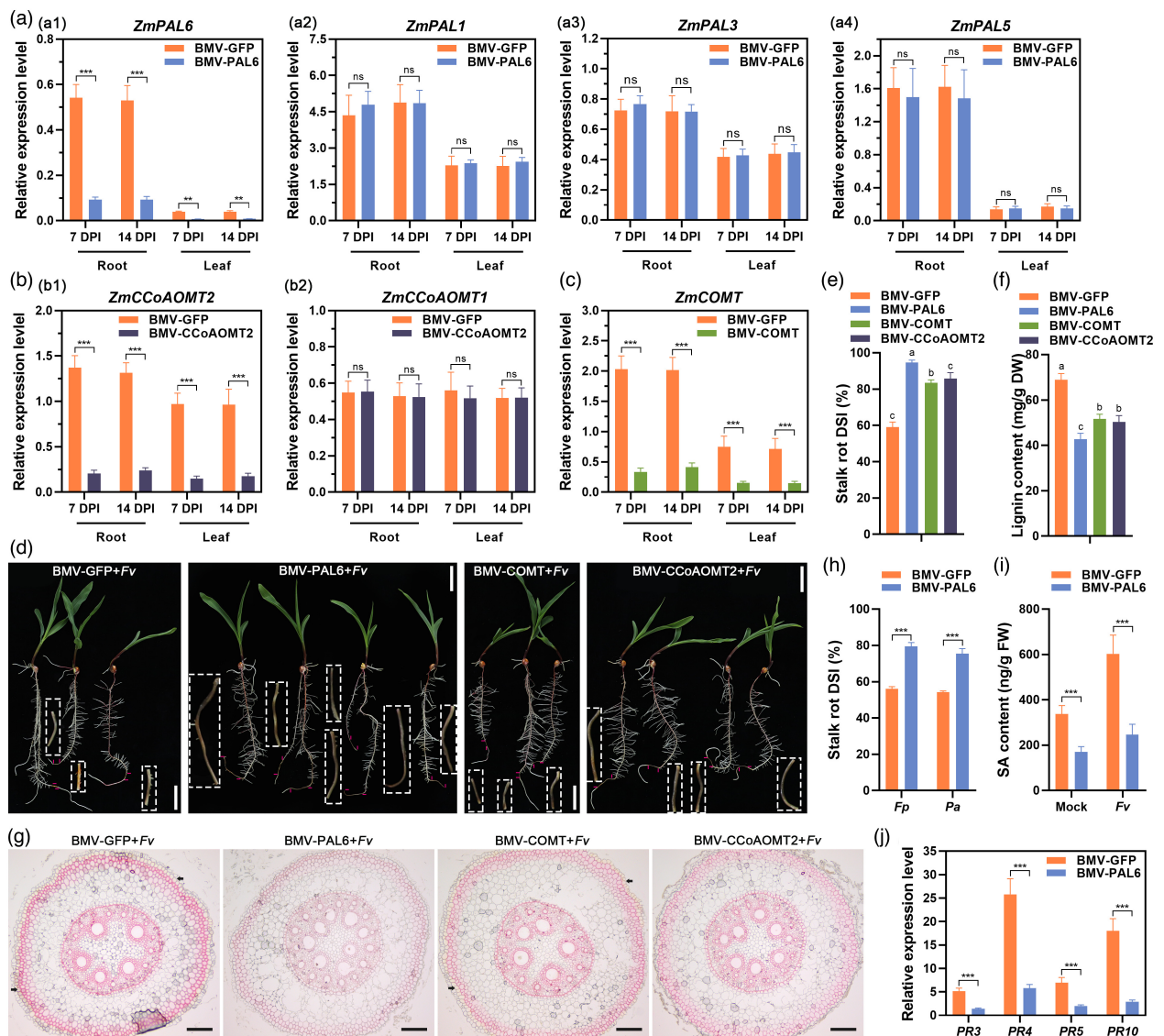


Figure 6 Phenylpropanoid pathway-related genes participate in *Fv* defense in several types of root cells. (a–e) Knockdown of expression of phenylpropanoid pathway-related genes in maize plants through BMV (brome mosaic virus)-mediated VIGS (virus-induced gene silencing) facilitates *Fv* infection. Silencing efficiency and specificity of *ZmPAL6* (a1 to a4), *ZmCCoAOMT2* (b1, b2), and *ZmCOMT* (c) in *Fv* infected leaves and roots were measured at 7 and 14 dpi, respectively. At 7 dpi, the BMV-GFP and chimeric BMV-CP5 inoculated cv. Va35 seedlings were challenged with *Fv*, the inoculated seedling roots were recorded for symptoms in the disease region at 48 hpi (d), and stalk rot DSI for *Fv*-inoculated maize seedling roots (e). Scale bars = 4 cm in (d). (f) Transient silencing of *ZmPAL6*, *ZmCOMT*, and *ZmCCoAOMT2* impairs the lignin accumulation in *Fv*-infected maize plants. (g) The histochemical localization of lignin in the *ZmPAL6*-, *ZmCOMT*-, and *ZmCCoAOMT2*-silenced seedling roots after *Fv* infection. Transverse ultrathin slices were prepared from the lower-root segments immediately adjacent to the lesions and then subjected to Maule staining. Red-purple staining in the cells of hypodermal layers and vascular cylinder indicates the presence of S-unit lignin. The outermost layer just below the epidermis is stained brown, indicating G-unit lignin (arrow). Scale bars = 100 µm. (h) The stalk rot DSI of the *ZmPAL6*-silenced maize seedling roots that were inoculated with stalk rot fungal pathogens *Fusarium proliferatum* (*Fp*) and *Pythium aristosporum* (*Pa*) at 48 hpi. (i–j) Knockdown of expression of *ZmPAL6* reduced salicylic acid (SA) accumulation and repaired expression of SA-regulated genes. Samples were harvested from *ZmPAL6*-silenced and *Fv*-infected maize plants, and BMV-GFP pre-inoculated and *Fv*-infected plants at 48 hpi and further used to measure SA content (i) and detect expression of pathogenesis-related (PR) genes (j). For (a–j) except (d and g), values are means ± SD. ***P < 0.001 (according to a paired Student's t-test) and NS, not significant. Different letters on the columns show significant differences (P < 0.05) (e and f) as determined by Tukey–Kramer test.

plant defence hormone with critical roles in pathogen-associated molecular pattern (PAMP)-triggered immunity (PTI), ETI, and systemic acquired resistance (SAR) (Zhang and Li, 2019), and the isochorismate synthase (ICS) pathway is

responsible for basal and pathogen-induced SA accumulation in plants (Qi et al., 2018; Torrens-Spence et al., 2019; Wu et al., 2022). For the M4 and M5 (Figure 4b) joint immune network, ICS-SA biosynthesis-related genes seem to be the key

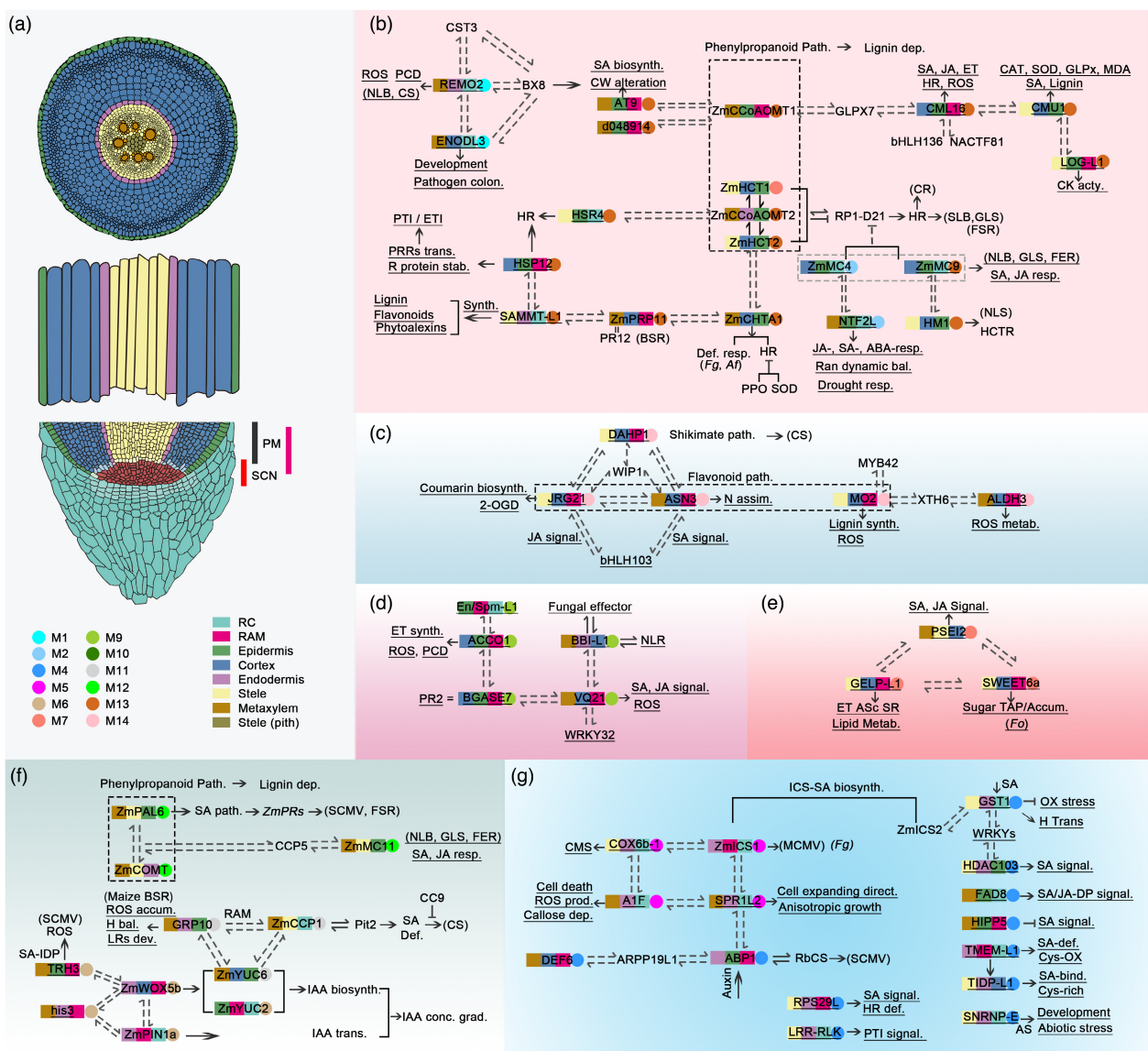


Figure 7 Construction of cell type-specific immune regulatory networks in maize roots. (a) Schematic diagram of transverse and longitudinal sections of maize primary root tip. Different colors of rectangle and circular denote specific cell types and gene co-expression modules, respectively. Based on our regulatory analyses, known resistance genes and QTL/QTN-predicted genes that are associated with *Fv* challenge can be assigned to cell identity or cell type-specific immunity regulatory networks. (b) The phenylpropanoid pathway-related immune regulatory network through integrating the M1 (RC_Qi319_MK/Fv), M2 (RC_B104_MK/Fv), and M13 (Epidermis_Qi319_Fv) modules. (c) The cortex-specific flavonoid pathway-related immune network based on the M14 (Cortex_Qi319_Fv) module. (d) The immune network of cortex/metaxylem two cell types based on the M9 module (Cortex/Metaxylem_B104_Fv). (e) The stele-specific immune network based on the M7 module (Stele_B104_MK/Fv-Qi319_Fv). (f) The crosstalk between the IAA-mediated disease resistance and SA-related defense pathways based on the RAM-specific M6 (RAM_B104_MK/Fv-Qi319_Fv), metaxylem-specific M11 (Metaxylem_Qi319_Fv) and M12 (Metaxylem_B104_MK/Fv) modules. (g) The interplay of the M4 (Endodermis_B104_MK/Qi319_Fv) and M5 (RC_Qi319_Fv) modules. Known maize resistance genes, QTL/QTN-predicted genes (underlined) associated with resistance to *Fv* and other pathogens, cell types with the top three expression abundance among the seven main cell types, and specific co-expression modules are indicated with different colors. The pathways or biological functions of known resistance genes are displayed, while the possible pathways or biological functions of QTL/QTN-predicted genes are labeled by underlining. The known resistance genes-associated diseases or pathogens are listed in the brackets. The two-way arrows indicate the known interactions, whereas the double-way dashed arrows illustrate the interplays predicted by the GENIE3. The details of the abbreviations in this figure are available in Appendix S2.

factors in this network, and the enriched genes are associated with SA signalling, ROS production, and removal, HR, cell development, defensive-metabolites deposition, and PTI launching (Figure 7g).

Taken together, these six integrated regulatory networks, consisting of the known and predicted disease-related genes, their cell types in root tips, disease-resistance signalling or metabolic pathways, and regulatory connections, provide insights

into the immune response mechanisms of major cell types in maize root tips at single-cell resolution.

Discussion

A comprehensive single-cell atlas of maize root tips provides the feasibility to construct cell type-specific regulatory networks in maize roots

Under the projected future global warming, the epidemic of plant diseases caused by soil-borne pathogens is expected to rise at a global scale (Delgado-Baquerizo *et al.*, 2020). A better understanding of the genetic disease-resistance potentials and regulatory mechanisms underlying immune responses in plant roots is indispensable to drawing up new strategies to control the diseases. Here, we reported a comprehensive single-cell atlas of maize root tips in two inbred lines and identified 21 cellular clusters and seven major cell types by using our defined cell markers, RNA *in situ* hybridization, and relative information reported previously. The number of cell clusters and cell types observed in our study were largely consistent with a published study of maize root scRNA-seq (Ortiz-Ramírez *et al.*, 2021). Among our defined cell markers, 856 marker genes including 24 makers, such as *Zm00001d049683*, *Zm00001d017508*, *Zm00001d003707*, *alpha carbonic anhydrase 7* that were validated using RNA *in situ* hybridization showed the same cell types as previous reports (Figure 2f, Figure S3, Tables S3, S11). Notably, the cell types of 68 marker genes (e.g., *aberrant pollen transmission1*, *NAC131*, *CCP5*, *phytosulfokine peptide precursor1*) reported here were perfectly consistent with both two published studies (Table S3) (Li *et al.*, 2022; Ortiz-Ramírez *et al.*, 2021). Intriguingly, we also identified cluster 14 as pith (a sub-stele cell type) according to RNA *in situ* hybridization of marker gene *Zm00001d051333* (Figure S3g,h). Thus, marker genes of cluster 14 could be used for identifying root pith cells in future. Compared with previous studies (Li *et al.*, 2022; Marand *et al.*, 2021; Ortiz-Ramírez *et al.*, 2021), the cell types of root tips identified here were validated by RNA *in situ* hybridization, these identified cell-type-specific marker genes can be thus used for cell sorting to generate high-quality cell-type-specific transcriptomes of maize root tips.

With the aid of WGCNA and GENIE3, a comprehensive single-cell atlas of maize root tips provides the feasibility to dissect cell type-specific regulatory networks in maize roots. The QTL- and QTN-predicted maize disease-related genes and known disease resistance-related genes were creatively selected through the bibliometric and integrated bioinformatics analyses of maize disease resistance-related publications as described previously (Wang *et al.*, 2023; Wei *et al.*, 2022). These genes were compared with 4049 *Fv*-responsive DEGs from scRNA-seq data, and then 148 overlapped genes were found to be harboured in *Fv*-induced co-expression modules with specific cell types (Figure 4b; Figure S5f). Among them, we found that RAM-specific *ZmWOX5b* and *ZmPIN1a* genes protect RAM free from *Fv* infection through coordinating the nonuniform distribution of IAA in root tips (Figure 5h,i). In addition, *ZmPAL6*, *ZmCOMT*, and *ZmCCoAOMT2* are involved in the defence responses against *Fv* by regulating lignin deposition in root cell walls upon the fungal attack (Figure 6). Notably, these three genes take effect in different cell types. Knocked-down expression of *ZmCOMT* leads to a drastic decrease of lignin content and lignin staining in three to four cell layers of hypodermal cells, vascular cylinder, and endodermis (Figure 6g), and these regions not including the

outmost hypodermal layer cells were lignified with syringyl (S) units (Guillaumie *et al.*, 2007). *ZmCCoAOMT2*, similar to *ZmCOMT*, acts downstream in monolignol biosynthesis (Osakabe *et al.*, 1999; Parvathi *et al.*, 2001), and appears to be more important for the constitutive lignification in the outermost layer of hypodermal cells (Figure 6g), which is deposited with guaiacyl (G) units of lignin polymers (Guillaumie *et al.*, 2007). Similarly, the lignin was histochemically stained at low levels in all lignified cell types (hypodermal cells, vascular cylinder, and endodermis) of the *ZmPAL6*-silenced roots (Figure 6g), suggesting that *ZmPAL6* is involved in the upstream regulatory pathway of lignin biosynthesis (Yadav *et al.*, 2020). These results prove that the phenylpropanoid pathway-related genes can regulate lignin deposition in different types of cells through their cell-specific regulatory networks (Figures 4b and 7b,f).

Immune networks uncover the overlapping of global host responses in maize roots post fungal infection

Plants have evolved two sensory mechanisms to identify pathogen invasions. One is the cell surface-located pattern recognition receptors (PRRs) sensing the conserved microbial elicitors called PAMPs to initiate PTI (Chisholm *et al.*, 2006; DeFalco and Zipfel, 2021). The second class of perception involves direct or indirect recognition by intracellular receptors of pathogen virulence molecules called effectors, and this recognition initiates ETI (Cui *et al.*, 2015; Jones and Dangl, 2006). Several cellular events are associated with both PTI and ETI and include a rapid activation of mitogen-activated protein kinases (MAPKs) and calcium-dependent protein kinases (CDPKs) signalling, ROS burst and scavenging, defence hormones signalling, biosynthesis and deposition of defensive-related metabolites (such as lignin, phytoalexin, coumarins, callose, and others), epigenetic regulation of gene expression, and localized cell death (Dodds and Rathjen, 2010). Considering that root performance is decided by the synergistic action of different root cells, we undertook a cell type-specific transcriptome analysis to identify regulatory networks in different type cells of maize roots challenged with *Fv* (Figure 4). On this foundation, the immune regulatory networks constructed here provide a global scene of PTI- and ETI-associated signalling pathways and downstream immune responses (Figure 7, Table S10). Notably, these immune regulatory networks were confirmed by phenotypic changes of plant defence-related physiological and biochemical characteristics in two inbred lines post *Fv* inoculation (Figure 1i,k, Figure S1i). In addition, there is an extensive overlap of the SA-signalling pathway among these immune regulatory networks (Figure 7b,d-h), being consistent with previously published results (Herrera-Vásquez *et al.*, 2015; Radojčić *et al.*, 2018; Wang *et al.*, 2021), demonstrating the feasibility of these constructed immune regulatory networks.

By combining WGCNA with GENIE3 analyses, we identified distinct regulatory patterns among these immune regulatory networks in a cell type-specific manner (Figures 4b and 7) and found that they were efficient for elucidating regulatory networks of DEGs. For example, a TF gene *MYB42*, a target of three key regulators (*MO2*, *ASN3*, and *JRG21*) (Figure 4b, Table S9), which was involved in the cell wall structure by repressing genes of the lignin pathways (Sonbol *et al.*, 2009), was also predicted to be associated with lignin synthesis through GENIE3 method (Figure 7c). Other TF target genes, belonging to WRKY, bHLH, and NAC families which were reported to be important factors in

plant-pathogen interactions (Amorim *et al.*, 2017; Campos *et al.*, 2022), were found to associate with defence hormone signalling, ROS burst, and HR defence (Figure 7b–d,g), indicating the accuracy of our prediction tool to reveal the interplay among cell type-specific regulatory networks.

Cell type-specific immunity networks in maize roots lay foundation for dissecting the underlying mechanisms of disease resistance

Our findings that root cell types keep their identity under *Fv* infection, as indicated by expression patterns of cell-type marker genes and regulation of cell identity genes under *Fv* infection (Figures 4b and 7; Figure S5a,b), indicated the interplay of cell identity and cell type-specific immune regulatory networks. Our experimental data (Figures 5 and 6) and the constructed immune regulatory networks (Figure 7b–g) suggest a close interdependency between developmental and disease-resistance networks through the perception (receptor) to hormones signalling transduction to adjust overall root development in responsive to fungal stimuli. The interaction of cell identity and cell type-specific immune networks enriches regulatory mechanisms at the gene level to support this crosstalk of plant development-environment interface. These findings demonstrate the complexity of immunity signalling in maize roots conditioning fungal invasion. Genes selected for the construction of cell-type specific immunity networks are associated with the main diseases of maize (Table S10), thus these defence pathways would likely apply to exploring immune responses and disease-resistance mechanisms against pathogens through verifying these gene functions by using gene editing and gene overexpression technologies as described previously in maize (An *et al.*, 2020; Jiang *et al.*, 2021; Liu *et al.*, 2022; Wan *et al.*, 2021).

By combining the cell type-specific transcriptomes and experimental validation, we constructed six cell type-specific immune regulatory networks in responsive to *Fv* infection. This study provides not only a global view of maize cell fate determination during root development but also insights into the immune regulatory networks in major cell types of maize root tips at single-cell resolution, thus laying the foundation for dissecting molecular mechanisms underlying disease resistance in maize.

Materials and methods

Plant materials and pathogenic fungi

The seeds of maize stalk rot-resistant inbred line Qi319 were kept in our lab, and that of the susceptible line B104 were kindly provided by Dr. Hallauer at Iowa State University. Seeds of cv. Va35 plants that were used for brome mosaic virus (BMV) inoculation were got from the University of Nebraska, Lincoln.

The causal agents of maize stalk rot including *Fv* (isolate #17FV), *F. proliferatum* (*Fp*) (isolate #24-3-1), and *Pythium aristosporum* (*Pa*) (isolate #T2) were isolated from the infected maize stem tissues and the colonies were single-spore subcultured on PDA (BD Difco™ Potato Dextrose Agar, Sparks, MD) media at 25 °C for 7 days and harvested for inoculum preparation.

Protoplasts isolation

An efficient protocol for isolation of maize root protoplasts with high viability including sections of (i) maize seed germination and seedling growth, (ii) protoplasts isolation and purification, and (iii)

protoplast counting and viability assessment are available in Appendix S1 section of the Supporting Information.

Artificial inoculation of maize seedlings

On the morning of the eighth day, the germination paper was unrolled and the seedling growth status was evaluated. The healthy plants were used for the following artificial inoculation experiment. Every eight seedlings were transferred into 250 mL 1/2 MS media (M5524, Sigma, Saint Louis, MO) poured in a 24 × 24-cm culture dish (BioSharp Life Sci, Beijing, China). Maize roots were placed on the surface of the medium before the infection (Figure S1c). The inoculum was achieved by homogenization of five plates of flourish hyphal mats (approximately 125 mL) with a kitchen blender and adjusted to a final volume of 200 mL with sterilized ddH₂O. Then the root tips were challenged with 20 µL of the mycelia plug inocula, mock-inoculated maize roots treated with PDA plug served as the control (Figure S1d). The root systems were covered with a sheet of germination paper wetted with liquid 1/2 MS media (Figure S1e). Subsequently a piece of aluminium foil was used to maintain moisture and avoid light exposure and contamination from other potential organisms (Figure S1f). Finally, the culture dish was covered with its lid or the zip block bag (BioSharp) and transferred into the growth cabinet for another 48 h with the above-mentioned growth condition (Figure S1g).

Disease symptoms evaluation

Roots of the inoculated seedlings were scored at the disease regions at 24 h postinoculation (hpi) or 48 hpi with a rating grade of 1–5 as previous description (Ye *et al.*, 2019). Two parameters were used to evaluate the symptoms, the first one was stalk rot score on average (SRSA) = $\sum \text{SRS}/n$. The second one was [Disease severity index (%)] (DSI) = $\sum (\text{grade} \times \text{number of plants in grade}) \times 100/(5 \times \text{total number of plants})$.

Physiological and biochemical characteristics measurement

To assay the physiological and biochemical characteristics related to plant defence reaction post fungal inoculation, roots, and leaves of the two inbred lines were harvested at 0, 12, 24, 36, and 48 hpi, respectively. The physiological and biochemical characteristics including hydrogen peroxide (H₂O₂) content (µmol/g), lipid peroxidation MDA (malondialdehyde) level (mmol/g), oxygen free radical (OFR) capacity (mmol/g), phenylalanine ammonia-lyase (PAL) activity (U/g), peroxidase (POD) activity (U/g), polyphenol oxidase (PPO) activity (U/g), catalase (CAT) activity (U/g), superoxide dismutase (SOD) activity (U/g), soluble saccharide concentration (mg/g), total protein concentration with BCA method (mg/g), lignin content (mg/g fresh weight) and the contents of chlorophyll (mg/g) were measured with the assay kits of Comin Biotechnology Co., Ltd (Suzhou, China) following the manufacturer's protocols.

scRNA-seq library construction and sequencing

Single-cell suspensions were loaded to 10x Chromium Controller to generate single-cell gel beads in emulsion according to the manufacturer's instructions for the 10x Genomics Chromium Single-Cell 3'kit (V3). Two independent replicates were performed. The following cDNA amplification and library construction steps were performed according to the standard protocol. Libraries were sequenced on an Illumina NovaSeq 6000

sequencing system (paired-end multiplexing run, 150 bp) by LC-Bio Technology Co. Ltd. (HangZhou, China).

Pre-processing of raw scRNA-seq data

The raw scRNA-seq dataset was analysed by Cell Ranger 3.1.0 (10x Genomics) and gene reads were aligned to the maize B73 reference genome (ftp://ftp.ensemblgenomes.org/pub/release-44/plants/fasta/zea_mays/dna/V4). For quality control, the low-quality cells and genes were filtered as follows: (1) the genes expressed in less than one cell were filtered out; (2) the number of expressed genes per cell above 500 was considered; (3) the cells with the percent of mitochondrial-DNA derived genes >25% were excluded.

Cell clustering and identification of marker genes

To visualize the data, we further reduced the dimensionality of all 29 217 cells using Seurat (Satija *et al.*, 2015) and t-SNE (Van der Maaten and Hinton, 2008) to project the cells into 2D space. The LogNormalize method of the Normalization function of the Seurat software was used to calculate the expression value of genes. Principal component analysis was performed using the normalized expression value, and the top 20 principal components were used to construct clustering and for t-SNE analysis. The weighted shared nearest neighbour graph-based clustering method was adopted to determine cell clusters.

Marker genes were selected using the following parameters: the genes were expressed in more than 10% of the cells in a cluster; the average \log_2 fold change of up-regulated genes was greater than 0.59 and the *P* value was smaller than 0.01. The selected marker genes were further validated using RNA *in situ* hybridization. Marker genes for each cluster were identified with the bimod (Likelihood-ratio test) with default parameters via the FindAllMarkers function in Seurat.

As cluster13 and cluster 18 are two independent clusters, the DEGs between them were calculated using the FindMarkers function. A significant DEG was defined if the $\Delta\log_2FCI$ was greater than 0.26, and the *P* value was <0.01. Genes with positive values of the \log_2FC represented higher expression levels in cluster 13 than that in cluster 18. Conversely, genes with negative values of \log_2FC were enriched in cluster 18. The DEGs between *Fv* and mock were also identified within each cell type according to the above criteria.

Bulk RNA-seq analysis

To evaluate the accuracy of scRNA-seq analysis, bulk RNA-seq analysis for root tips was performed with three replicates. To prepare the bulk RNA-seq samples, the 5 cm-long root tips, except the diseased region or mock-inoculated segments were harvested at 48 hpi. Total RNA was isolated and purified using TRIzol reagent (Invitrogen, Carlsbad, CA) following the manufacturer's procedure. We performed the 2×150 bp paired-end sequencing (PE150) on an Illumina Novaseq™ 6000 (LC-Bio Technology CO., Ltd., Hangzhou, China) following the vendor's recommended protocol. Sequence reads were trimmed using cutadapt (v1.9) and aligned to the maize B73 reference genome using HISAT2 (v2.0.4) (Kim *et al.*, 2019). Fragments per kilobase of exon model per million mapped reads were calculated using StringTie and ballgown (v1.3.4), and edgeR was used to calculate differential expression ($\Delta\log_2FCI \geq 1$ and *P* < 0.05) in response to *Fv* treatment (compared with mock).

Pseudotime analysis

Trajectory inference and pseudotime analysis were performed for selecting clusters using Monocle2 (Trappnell *et al.*, 2014). Briefly, high variable genes were first selected using the dispersionTable function and mean_expression function (≥ 0.1). The dimensional reduction clustering analysis was performed using the reduceDimension function (max_components = 2, reduction_method = DDTTree). The state transition of single cells was deduced by orderCells function with default parameters. The trajectory was visualized by plot_cell_trajectory in Monocle 2. Branched expression analysis modelling was performed to identify genes with branch-dependent expression. Gene expression along the branch point was clustered and plotted using plot_genes_branches_heatmap function.

Weighted gene co-expression network analysis (WGCNA) within cell types

The WGCNA package (Langfelder and Horvath, 2008) in R software was used in co-expression analysis to detect relative relationships among genes with cell types of two genotypes under two treatments. A weighted adjacency matrix was created using an unsupervised hierarchical clustering method, and the soft threshold power (β) was set at 14 to analyse the scale-free topology. Modules were identified according to the following parameters: minModuleSize = 30, mergeCutHeight = 0.15. Significant co-expression modules were defined if the Pearson correlation coefficient was >0.40 and the *P* value was <0.05.

Gene regulatory network analysis using a machine-learning approach

A comprehensive bibliometric analysis of 226 publications was selected by the related queries of QTL mapping and GWAS analysis for maize disease-related traits. Totally 1976 QTLs and 4096 QTNs were identified. After QTL projection to physical position, the QTLs, QTNs, reported genes associated with disease resistance were combined for discovering the overlapped regions. QTL or QTN-predicted genes were compared against the scRNA-seq data and overlapped genes were found in significant co-expression modules for cell types. Finally, a gene regulatory network was constructed for these overlapped genes and known disease-related genes by using a random forest-based algorithm GENIE3 (Huynh-Thu *et al.*, 2010). These genes were used as regulators and their targets were revealed in significant *Fv*-related co-expression modules. The threshold of weight value was set at 0.10, and other parameters were set at default. The gene networks were conducted using the R package GENIE3 and visualized using Cytoscape v3.9.1 (Shannon *et al.*, 2003).

GO and KEGG enrichment analysis

Enrichment analyses were performed using the OmicStudio tools (<https://www.omicstudio.cn/tool>). Significant GO terms and KEGG pathways were defined if the *P* value was small than 0.05.

RNA *in situ* hybridization

The wild-type and transgenic maize roots were collected for the preparation of the transverse ultrathin sections and longitudinal slices. The plant material was fixed in 4% paraformaldehyde (Sigma) in 0.1 M phosphate buffer (pH 7.2) for 16 h at 4 °C, then dehydrated by ethanol series and embedded in Paraplast Plus (Sigma). Sections (7–10 µm) were cut using a Leica RM 2135 microtome (Leica, Germany) and collected on xylene-coated

SuperFrost Plus slides (Menzel-Gläser, Thermo Scientific, Waltham, MA). Slides were then deparaffinized and treated with 10 µg/mL proteinase K.

Add pre-hybridizing solution to each section and incubate for 1 h at 37 °C. Remove the pre-hybridization solution, incubate in the hybridizing solution containing 1 µM of DIG-labelled probes at 42 °C overnight. At 37 °C, wash the slices with 2× SSC buffer for 10 min, with 1× SSC for 5 min two times; then wash with 0.5× SSC for 10 min at room temperature. Then the slices were incubated in the blocking solution (rabbit serum) at room temperature for 30 min. Discard the blocking solution, and add the alkaline phosphatase-conjugated IgG fraction monoclonal mouse anti-Digoxin antibody (anti-DIG-AP), incubate at 37 °C for 50 min, wash the sections with TBS buffer four times, each time 5 min. Blot up the slides carefully, add freshly prepared NBT/BCIP chromogenic reagent to mark the tissue. Manage the reaction time by microscopic observation of the reaction, it could be terminated till the appearance of the blue-purple or similar colour. Slides were air-dried and mounted with DPX slide mounting medium (Sigma). Image the results using a bright field fluorescence microscope. More information on the probes for each gene can be found in Table S11.

Maize transformation and events analysis

To construct *ZmWOX5b*, *ZmPIN1a* enhance-expression (EE) binary constructs for functional validation, the DNA fragment containing the native *ZmWOX5b* (*ZmPIN1a*) gene with promoter, coding sequence and the *GFP* gene open reading frame were amplified utilizing homologous recombination primer pairs (Table S12). The amplified fragment was inserted into the binary vector pFGC5941 (Kerschen et al., 2004) (Figure S7a,b). For the construction of *ZmWOX5b* (*ZmPIN1a*)-RNAi vector, gene-specific fragments were amplified and successively fused in a way of head-to-head into the flanking regions of the CHS intron of the pFGC5941, respectively (Table S12, Figure S7g,h).

The maize transformation and events analysis were conducted in the Plant Transformation Core Facility of the University of Missouri-Columbia using our optimized protocols derived from the previous protocol (Frame et al., 2006). The plasmids of the binary constructs were introduced into the maize inbred line B104 immature embryos via *Agrobacterium tumefaciens* (strain AGL1) mediated transformation.

To determine the segregation of the gene of interest (RNAi insert) and selectable marker gene, at least 20 plants from each *T*₀ event were screened using PCR and leaf-painting analysis with 500 mg/L glufosinate prepared from Liberty® (Aventis Crop Science, St Louis, MO). Chi-squared test was used to analyse the segregation ratios of bar and gene of interest (RNAi insert) of *T*₁ plants based on herbicide resistance and PCR, respectively. *T*₂ progenies from the *T*₁ generation were similarly analysed to identify homozygous *T*₁ lines for subsequent study.

For Southern blotting analysis, genomic DNA was extracted from the transgenic B104 plants following a modified CTAB-based protocol. A total of 30 µg of genomic DNA was digested with restriction enzyme *Bam*H1, which cuts only once within the T-DNA of plasmids pFGC5941, DNA fragments were fractionated on a 1.0% agarose gel before transferring to Zeta-Probe® GT nylon membrane (Bio-Rad, CA). DNA was fixed to the membrane by UV cross-linking. Hybridization and membrane washing was conducted at 65 °C according to the manufacturer's instructions. Prime-It® RmT Random Primer Labeling Kit (Stratagene, La Jolla, CA) was used to generate ³²P-labelled probes of target genes or

RNAi inserts obtained from PCR-amplified using primers listed in Table S12.

Virus-induced gene silencing

An improved brome mosaic virus (BMV) silencing vector (Ding et al., 2018) was used to knock down the target genes. Sequence-specific DNA fragments representing the *ZmPAL*, *ZmCOMT*, and *ZmCCoAOMT2* genes, were amplified from a maize cv. Va35 root cDNA using specific primer pairs (Table S12) and ligated into the pC13/F3CP5 RNA3, respectively. A control RNA3 vector plasmid containing a 250-bp insert from a variant of the GFP gene, to produce pC13/F3CP5: GFP (Ding et al., 2018).

Agrobacterium tumefaciens cultures carrying pC13/F3CP5: PAL, pC13/F3CP5:COMT, pC13/F3CP5:CCoAOMT2 or pC13/F3CP5:GFP were prepared and infiltrated into *Nicotina benthamiana* leaves as previously described (Ding et al., 2018; Zhu et al., 2014).

BMV virion was isolated from the agroinfiltrated *N. benthamiana* leaves and inoculated into 8-d-old maize cv Va35 seedlings, as previously described (Ding et al., 2018; Zhu et al., 2014). The inoculated maize plants were grown inside a growth chamber set at 20 °C and 16 h of light and 8 h of dark for 7 day before transferring to 1/2 MS media for artificial inoculation and phenotype observations. The cv. Va35 seed germination, seedling growth (except the first 7 day after BMV inoculation), artificial inoculation, and disease severity evaluation were identical to the relevant section, as described above.

Total RNA was isolated from the second and third systemically infested leaves and the roots of individual Va35 plants pooled at 7 and 14 dpi, and subjected to RT-qPCR for gene silencing efficiency and specificity analysis.

Real-time quantitative RT-PCR

Total RNA was purified from different samples using TRIzol reagent (Invitrogen) according to the manufacturer's protocols, and treated with RNase-free DNase I (TaKaRa, Dalian, China) to remove potential contaminating DNA. The first-strand cDNA was synthesized using 2.0 µg of total RNA per 20 µL reaction with SuperScript™ III Reverse Transcriptase (Invitrogen) and random hexamer primers.

Ten-fold diluted cDNA, a set of gene-specific primers (listed in Table S12), and SYBR Green Master mixture (Applied Biosystems Inc., Foster City, CA) were mixed for quantitative RT-PCR (qPCR) to determine the transcript levels of the genes on an ABI 7500 Real-Time PCR system (Applied Biosystems). Templates were normalized with *ZmTub4* as a control. The relative expression level of each gene was calculated using the 2^{-ΔΔCT} method (Livak and Schmittgen, 2001). Each expression analysis was carried out for at least three biological replicates, with three technical replicates for each biological replicate. The primers used in the real-time qRT-PCR were listed in Table S12.

WGA staining

At 24 and 48 hpi, the roots of wild type Qi319 and B104 seedlings that inoculated with *Fv* were cut above the meristem at nearly 10–12 mm from the root tip and subjected to the preparation of 5 µm-thick longitudinal slitting slices; whereas for the free-hand transverse sections, slices of approximately 5 µm were acquired at approximately 7 mm, 12 mm from the tip, respectively. For the *ZmWOX5b*, *ZmPIN1a* transgenic plants, approximately 7 mm-in length root tips were collected at 24 hpi

and used for the longitudinal slices making to monitor the growth of fungal hyphae.

The samples were then co-stained with wheat-germ agglutinin-Alexa Fluor 488 conjugate (WGA-AF488) and propidium iodide (PI) (Redkar et al., 2018). WGA-AF88 stains fungal hyphae green, and the propidium iodide stains plant cell walls red. After staining, the slides were scanned and digitalized by using a Pannoramic MIDI II (3DHISTECH, Budapest, Hungary) with differential epifluorescence (GFP filter set for WGA-AF488: 450–490 nm excitation, 500–550 nm emission; TX2 filter set for PI: excitation 540–580 nm, emission 608–683 nm). The image was analysed using the program, Pannoramic Viewer (3D HISTECH).

The signals of WGA-AF488 were analysed with Image-Pro Plus 6.0 (Media Cybernetics, Rockville, MD) to evaluate the longitudinal migration of *Fv* by measuring the distance between the root tip and the hyphae (DTH) advancing frontline. The WGA signals of the longitudinal slices and cross sections were evaluated by measuring the area density of the green fluorescence. Area density indicates IOD (Integrated optical density) of the WGA signal per area.

Microscopy

Counting of total and viable protoplasts was performed with the ordinary optical microscope (Leica, Wetzlar, Germany) and fluorescent microscope (OLYMPUS Model BX61, Tokyo, Japan), respectively. GFP fluorescence observations were made using a Leica M205 FA stereomicroscope supplied with a DFC 7000T camera with GFP filter excitation wavelengths 470–540 nm, emission wavelengths 525–550 nm, and the magnification 10–40 \times with different filters suitable for the spectrum of 450–490 nm in excitation of GFP for maize.

Auxin content measurement

The roots were collected from the young transgenic siblings vertically grown in a growth chamber. These roots were divided into specific segments, which were labelled from A to E indicating the segment A (RC, root cap), B (RAM, root apical meristem), C (TZ, transition zone), D (EZ), and E (MZ; mature zone), as shown in Figure 5*i*. Endogenous IAA was extracted from the segments and quantified by GC–MS in selected ion monitoring mode (GC-SIM-MS), refer to Nishimura et al. (2014) for details. Samples from three biological replicates were quantified individually.

Lignin histochemical staining

Maize root samples (upper-root segments immediately adjacent to the diseased root regions) were collected and immediately frozen in liquid nitrogen. Transverse ultrathin sections were prepared with a Leica CM 1850 cryostat at –20 °C (Leica Microsystems Inc., Buffalo Grove, IL). Transverse samples were then subjected to Maüle reactions according to previously described protocols (Nakano and Meshitsuka, 1992). Images were captured by using a CCD camera (Colour Coolview; Photonic Science, Milham, UK) attached to an inverted microscope (Leitz DMRIE; Leica Microsystems, Wetzlar, Germany).

Acknowledgement

This work was supported by grants from the National Key Research & Development Program of China (2021YFD1200700; 2022YFF1003500; 2016YFD0100103) and the Agricultural Science and Technology Innovation Program of the Chinese Academy of Agricultural Sciences (CAAS-ASTIP-2017-ICS). We

thank Professor Richard S. Nelson (Plant Biology Division, The Samuel Roberts Noble Foundation Inc., OK) for providing the BMV-based VIGS vector.

Conflicts of interest

The authors declared that they have no conflict of interest.

Author contributions

Y.C., X.W., and C.D. conceived and designed the study. Y.C., S.H., M.H., and Z.Z. performed the experiments. J.M., X.Wei., and X.Z. performed bioinformatics analysis. Y.C., Y.L., Z.D., and L.K. analysed the data. S.S., X.Z., Z.Zhu, X.Wang and L.Z. participated in some experiments. Y.C., J.M., X.W., and C.D. wrote the manuscript. X.W., C.D., J.T., and X.L. revised the manuscript with feedback from all other authors.

Data availability statement

The raw scRNA-seq data are available at the SRA database of NCBI with accession No. PRJNA865791, and bulk RNA data that support the findings of this study have been deposited into the CNGB Sequence Archive (CNSA) of China National GeneBank DataBase (CNGBdb) with accession number CNP0003317.

References

- Amorim, L.L.B., da Fonseca Dos Santos, R., Neto, J.P.B., Guida-Santos, M., Crovella, S. and Benko-Iseppon, A.M. (2017) Transcription factors involved in plant resistance to pathogens. *Curr. Protein Pept. Sci.* **18**, 335–351.
- An, X., Ma, B., Duan, M., Dong, Z., Liu, R., Yuan, D., Hou, Q. et al. (2020) Molecular regulation of ZmMs7 required for maize male fertility and development of a dominant male-sterility system in multiple species. *Proc. Natl. Acad. Sci. USA*, **117**, 23499–23509.
- Campos, M.D., Félix, M.D.R., Patanita, M., Materatski, P., Albuquerque, A., Ribeiro, J.A. and Varanda, C. (2022) Defense Strategies: The role of transcription factors in tomato-pathogen interaction. *Biology (Basel)*, **11**, 235.
- Chen, H., Yin, X., Guo, L., Yao, J., Ding, Y., Xu, X., Liu, L. et al. (2021) PlantscRNAdb: A database for plant single-cell RNA analysis. *Mol. Plant*, **14**, 855–857.
- Cheng, S., Tan, F., Lu, Y., Liu, X., Li, T., Yuan, W., Zhao, Y. et al. (2018) WOX11 recruits a histone H3K27me3 demethylase to promote gene expression during shoot development in rice. *Nucleic Acids Res.* **46**, 2356–2369.
- Chisholm, S.T., Coaker, G., Day, B. and Staskawicz, B.J. (2006) Host-microbe interactions: shaping the evolution of the plant immune response. *Cell*, **124**, 803–814.
- Cui, H., Tsuda, K. and Parker, J.E. (2015) Effector-triggered immunity: from pathogen perception to robust defense. *Annu. Rev. Plant Biol.* **66**, 487–511.
- DeFalco, T.A. and Zipfel, C. (2021) Molecular mechanisms of early plant pattern-triggered immune signaling. *Mol. Cell*, **81**, 4346.
- Delgado-Baquerizo, M., Guerra, C.A., Cano-Díaz, C., Egidi, E., Wang, J.-T., Eisenhauer, N., Singh, B.K. et al. (2020) The proportion of soil-borne pathogens increases with warming at the global scale. *Nat. Clim. Change*, **10**, 550–554.
- Denyer, T., Ma, X., Klesen, S., Scacchi, E., Nieselt, K. and Timmermans, M.C.P. (2019) Spatiotemporal developmental trajectories in the *Arabidopsis* root revealed using high-throughput single-cell RNA sequencing. *Dev. Cell*, **48**, 840–852.e845.
- Ding, X.S., Mannas, S.W., Bishop, B.A., Rao, X., Lecoultrre, M., Kwon, S. and Nelson, R.S. (2018) An improved bromegrass mosaic virus silencing vector: greater insert stability and more extensive VIGS. *Plant Physiol.* **176**, 496–510.
- Dodds, P.N. and Rathjen, J.P. (2010) Plant immunity: towards an integrated view of plant-pathogen interactions. *Nat. Rev. Genet.* **11**, 539–548.

- Duan, C., Cao, Y., Dong, H., Xia, Y., Li, H., Hu, Q., Yang, Z. et al. (2022) Precise characterization of maize germplasm for resistance to *Pythium* stalk rot and *Gibberella* stalk rot. *Sci. Agric. Sin.* **55**, 265–279.
- Frame, B.R., McMurray, J.M., Fonger, T.M., Main, M.L., Taylor, K.W., Torney, F.J., Paz, M.M. et al. (2006) Improved *Agrobacterium*-mediated transformation of three maize inbred lines using MS salts. *Plant Cell Rep.* **25**, 1024–1034.
- Gai, X., Dong, H., Wang, S., Liu, B., Zhang, Z., Li, X. and Gao, Z. (2018) Infection cycle of maize stalk rot and ear rot caused by *Fusarium verticillioides*. *PLoS ONE*, **13**, e0201588.
- Garay-Arroyo, A., De La Paz Sánchez, M., García-Ponce, B., Azpeitia, E. and Alvarez-Buylla, E.R. (2012) Hormone symphony during root growth and development. *Dev. Dyn.* **241**, 1867–1885.
- Guillaumie, S., San-Clemente, H., Deswarthe, C., Martinez, Y., Lapierre, C., Murigneux, A., Barrière, Y. et al. (2007) MAIZEWALL. Database and developmental gene expression profiling of cell wall biosynthesis and assembly in maize. *Plant Physiol.* **143**, 339–363.
- Herrera-Vásquez, A., Salinas, P. and Holguigue, L. (2015) Salicylic acid and reactive oxygen species interplay in the transcriptional control of defense genes expression. *Front. Plant Sci.* **6**, 171.
- Huynh-Thu, V.A., Irrthum, A., Wehenkel, L. and Geurts, P. (2010) Inferring regulatory networks from expression data using tree-based methods. *PLoS ONE*, **5**, e12776.
- Jean-Baptiste, K., McFaline-Figueroa, J.L., Alexandre, C.M., Dorrity, M.W., Saunders, L., Bubb, K.L., Trapnell, C. et al. (2019) Dynamics of gene expression in single root cells of *Arabidopsis thaliana*. *Plant Cell*, **31**, 993–1011.
- Jiang, Y., An, X., Li, Z., Yan, T., Zhu, T., Xie, K., Liu, S. et al. (2021) CRISPR/Cas9-based discovery of maize transcription factors regulating male sterility and their functional conservation in plants. *Plant Biotechnol. J.* **19**, 1769–1784.
- Jin, J., Lu, P., Xu, Y., Tao, J., Li, Z., Wang, S., Yu, S. et al. (2022) PCMDB: a curated and comprehensive resource of plant cell markers. *Nucleic Acids Res.* **50**, D1448–D1455.
- Jones, J.D. and Dangl, J.L. (2006) The plant immune system. *Nature*, **444**, 323–329.
- Kang, H., Wu, D., Fan, T. and Zhu, Y. (2020) Activities of chromatin remodeling factors and histone chaperones and their effects in root apical meristem development. *Int. J. Mol. Sci.* **21**, 771.
- Kawa, D. and Brady, S.M. (2022) Root cell types as an interface for biotic interactions. *Trends Plant Sci.* **27**, 1173–1186.
- Kerschen, A., Napoli, C.A., Jorgensen, R.A. and Müller, A.E. (2004) Effectiveness of RNA interference in transgenic plants. *FEBS Lett.* **566**, 223–228.
- Kim, D., Paggi, J.M., Park, C., Bennett, C. and Salzberg, S.L. (2019) Graph-based genome alignment and genotyping with HISAT2 and HISAT-genotype. *Nat. Biotechnol.* **37**, 907–915.
- Kirschner, G.K., Stahl, Y., Von Korff, M. and Simon, R. (2017) Unique and conserved features of the barley root meristem. *Front. Plant Sci.* **8**, 1240.
- Langfelder, P. and Horvath, S. (2008) WGCNA: an R package for weighted correlation network analysis. *BMC Bioinform.* **9**, 559.
- Lee, M.H., Jeon, H.S., Kim, S.H., Chung, J.H., Roppolo, D., Lee, H.J., Cho, H.J. et al. (2019) Lignin-based barrier restricts pathogens to the infection site and confers resistance in plants. *EMBO J.* **38**, e101948.
- Li, J., Zhu, S., Song, X., Shen, Y., Chen, H., Yu, J., Yi, K. et al. (2006) A rice glutamate receptor-like gene is critical for the division and survival of individual cells in the root apical meristem. *Plant Cell*, **18**, 340–349.
- Li, X., Zhang, X., Gao, S., Cui, F., Chen, W., Fan, L. and Qi, Y. (2022) Single-cell RNA sequencing reveals the landscape of maize root tips and assists in identification of cell type-specific nitrate-response genes. *Crop J.* **10**, 1589–1600.
- Liu, S., Ma, H., Guo, N., Shi, J., Zhang, H., Sun, H. and Jin, G. (2019) Analysis of main pathogens and dominant species of maize stalk rot in the main summer maize producing areas of Huang-Huai-Hai. *Sci. Agric. Sin.* **52**, 262–272.
- Liu, Z., Zhou, Y., Guo, J., Li, J., Tian, Z., Zhu, Z., Wang, J. et al. (2020) Global dynamic molecular profiling of stomatal lineage cell development by single-cell RNA sequencing. *Mol. Plant*, **13**, 1178–1193.
- Liu, X., Zhang, S., Jiang, Y., Yan, T., Fang, C., Hou, Q., Wu, S. et al. (2022) Use of CRISPR/Cas9-based gene editing to simultaneously mutate multiple homologous genes required for pollen development and male fertility in maize. *Cell*, **11**, 439.
- Livak, K.J. and Schmittgen, T.D. (2001) Analysis of relative gene expression data using real-time quantitative PCR and the $2^{-\Delta\Delta CT}$ method. *Methods*, **25**, 402–408.
- Ma, Y., Miotk, A., Šutiković, Z., Ermakova, O., Wenzl, C., Medzhibradszky, A., Gaillotet, C. et al. (2019) WUSCHEL acts as an auxin response rheostat to maintain apical stem cells in *Arabidopsis*. *Nat. Commun.* **10**, 5093.
- Marand, A.P., Chen, Z., Gallavotti, A. and Schmitz, R.J. (2021) A cis-regulatory atlas in maize at single-cell resolution. *Cell*, **184**, 3041–3055.e3021.
- Marquez-Garcia, B., Njo, M., Beeckman, T., Goormachtig, S. and Foyer, C.H. (2014) A new role for glutathione in the regulation of root architecture linked to strigolactones. *Plant Cell Environ.* **37**, 488–498.
- Nakano, J. and Meshitsuka, G. (1992) The Detection of Lignin. In *Methods in Lignin Chemistry*(Lin, S.Y. and Dence, C.W., eds), pp. 23–32. Berlin, Heidelberg: Springer Berlin Heidelberg.
- Ning, Y. and Wang, G.L. (2018) Breeding plant broad-spectrum resistance without yield penalties. *Proc. Natl. Acad. Sci. USA*, **115**, 2859–2861.
- Nishimura, T., Hayashi, K., Suzuki, H., Gyohda, A., Takaoka, C., Sakaguchi, Y., Matsumoto, S. et al. (2014) Yucasin is a potent inhibitor of YUCCA, a key enzyme in auxin biosynthesis. *Plant J.* **77**, 352–366.
- Ortiz-Ramírez, C., Guillotin, B., Xu, X., Rahni, R., Zhang, S., Yan, Z., Coqueiro Dias Araujo, P. et al. (2021) Ground tissue circuitry regulates organ complexity in maize and *Setaria*. *Science*, **374**, 1247–1252.
- Osakabe, K., Tsao, C.C., Li, L., Popko, J.L., Umezawa, T., Carraway, D.T., Smeltzer, R.H. et al. (1999) Coniferyl aldehyde 5-hydroxylation and methylation direct syringyl lignin biosynthesis in angiosperms. *Proc. Natl. Acad. Sci. USA*, **96**, 8955–8960.
- Parvathi, K., Chen, F., Guo, D., Blount, J.W. and Dixon, R.A. (2001) Substrate preferences of O-methyltransferases in alfalfa suggest new pathways for 3-O-methylation of monolignols. *Plant J.* **25**, 193–202.
- Qi, G., Chen, J., Chang, M., Chen, H., Hall, K., Korin, J., Liu, F. et al. (2018) Pandemonium breaks out: disruption of salicylic acid-mediated defense by plant pathogens. *Mol. Plant*, **11**, 1427–1439.
- Radojičić, A., Li, X. and Zhang, Y. (2018) Salicylic acid: a double-edged sword for programmed cell death in plants. *Front. Plant Sci.* **9**, 1133.
- Redkar, A., Jaeger, E. and Doeblemann, G. (2018) Visualization of growth and morphology of fungal hyphae in planta using WGA-AF488 and propidium iodide co-staining. *Bio-protocol*, **8**, e2942.
- Rich-Griffin, C., Eichmann, R., Reitz, M.U., Hermann, S., Woolley-Allen, K., Brown, P.E., Wiwatdikul, K. et al. (2020) Regulation of cell type-specific immunity networks in *Arabidopsis* roots. *Plant Cell*, **32**, 2742–2762.
- Satija, R., Farrell, J.A., Gennert, D., Schier, A.F. and Regev, A. (2015) Spatial reconstruction of single-cell gene expression data. *Nat. Biotechnol.* **33**, 495–502.
- Satterlee, J.W., Strable, J. and Scanlon, M.J. (2020) Plant stem-cell organization and differentiation at single-cell resolution. *Proc. Natl. Acad. Sci. USA*, **117**, 33689–33699.
- Shannon, P., Markiel, A., Ozier, O., Baliga, N.S., Wang, J.T., Ramage, D., Amin, N. et al. (2003) Cytoscape: a software environment for integrated models of biomolecular interaction networks. *Genome Res.* **13**, 2498–2504.
- Shukla, V., Lombardi, L., Pencik, A., Novak, O., Weits, D.A., Loret, E., Perata, P. et al. (2020) Jasmonate signalling contributes to primary root inhibition upon oxygen deficiency in *Arabidopsis thaliana*. *Plants (Basel)*, **9**, 1046.
- Shulse, C.N., Cole, B.J., Ciobanu, D., Lin, J., Yoshinaga, Y., Gouran, M., Turco, G.M. et al. (2019) High-throughput single-cell transcriptome profiling of plant cell types. *Cell Rep.* **27**, 2241–2247.e2244.
- Sonbol, F.M., Fornalé, S., Capellades, M., Encina, A., Touriño, S., Torres, J.L., Rovira, P. et al. (2009) The maize ZmMYB42 represses the phenylpropanoid pathway and affects the cell wall structure, composition and degradability in *Arabidopsis thaliana*. *Plant Mol. Biol.* **70**, 283–296.
- Suzuki, H., Yokawa, K., Nakano, S., Yoshida, Y., Fabrisson, I., Okamoto, T., Baluška, F. et al. (2016) Root cap-dependent gravitropic U-turn of maize root requires light-induced auxin biosynthesis via the YUC pathway in the root apex. *J. Exp. Bot.* **67**, 4581–4591.

- Tamogami, S., Agrawal, G.K. and Rakwal, R. (2021) Fluorescent labeling of the root cap cells with the bioactive NBD-S chemical probe based on the cellulose biosynthesis inhibition herbicides. *Biochem. Biophys. Rep.* **27**, 101063.
- Thomann, A., Lechner, E., Hansen, M., Dumbliauskas, E., Parmentier, Y., Kieber, J., Scheres, B. et al. (2009) Arabidopsis *CULLIN3* genes regulate primary root growth and patterning by ethylene-dependent and -independent mechanisms. *PLoS Genet.* **5**, e1000328.
- Tian, H., Wabnik, K., Niu, T., Li, H., Yu, Q., Pollmann, S., Vanneste, S. et al. (2014) WOX5-IAA17 feedback circuit-mediated cellular auxin response is crucial for the patterning of root stem cell niches in *Arabidopsis*. *Mol. Plant*, **7**, 277–289.
- Torrens-Spence, M.P., Bobokalova, A., Carballo, V., Glinkerman, C.M., Pluskal, T., Shen, A. and Weng, J.K. (2019) PBS3 and EPS1 complete salicylic acid biosynthesis from isochorismate in *Arabidopsis*. *Mol. Plant*, **12**, 1577–1586.
- Trapnell, C., Cacchiarelli, D., Grimsby, J., Pokharel, P., Li, S., Morse, M., Lennon, N.J. et al. (2014) The dynamics and regulators of cell fate decisions are revealed by pseudotemporal ordering of single cells. *Nat. Biotechnol.* **32**, 381–386.
- Treutter, D. (2006) Significance of flavonoids in plant resistance: a review. *Environ. Chem. Lett.* **4**, 147–157.
- Van der Maatten, L. and Hinton, G. (2008) Visualizing data using t-SNE. *J. Mach. Learn. Res.* **9**, 2579–2605.
- Wan, X., Wu, S. and Li, X. (2021) Breeding with dominant genic male-sterility genes to boost crop grain yield in the post-heterosis utilization era. *Mol. Plant*, **14**, 531–534.
- Wang, L., Chu, H., Li, Z., Wang, J., Li, J., Qiao, Y., Fu, Y. et al. (2014) Origin and development of the root cap in rice. *Plant Physiol.* **166**, 603–613.
- Wang, C., Yang, Q., Wang, W., Li, Y., Guo, Y., Zhang, D., Ma, X. et al. (2017) A transposon-directed epigenetic change in *ZmCCT* underlies quantitative resistance to Gibberella stalk rot in maize. *New Phytol.* **215**, 1503–1515.
- Wang, X., Gao, J., Gao, S., Li, Z., Kuai, B. and Ren, G. (2019) REF6 promotes lateral root formation through de-repression of *PIN1/3/7* genes. *J. Integr. Plant Biol.* **61**, 383–387.
- Wang, Z., Rong, D., Chen, D., Xiao, Y., Liu, R., Wu, S. and Yamamoto, C. (2021) Salicylic acid promotes quiescent center cell division through ROS accumulation and down-regulation of *PLT1*, *PLT2*, and *WOX5*. *J. Integr. Plant Biol.* **63**, 583–596.
- Wang, S., Li, H., Dong, Z., Wang, C., Wei, X., Long, Y. and Wan, X. (2023) Genetic structure and molecular mechanism underlying the stalk lodging traits in maize (*Zea mays* L.). *Comput. Struct. Biotechnol. J.* **21**, 485–494.
- Wei, L., Zhang, W., Liu, Z. and Li, Y. (2009) AtKinesin-13A is located on Golgi-associated vesicle and involved in vesicle formation/budding in *Arabidopsis* root-cap peripheral cells. *BMC Plant Biol.* **9**, 138.
- Wei, X., Pu, A., Liu, Q., Hou, Q., Zhang, Y., An, X., Long, Y. et al. (2022) The bibliometric landscape of gene editing innovation and regulation in the worldwide. *Cells*, **11**, 2682.
- Wu, H., Qu, X., Dong, Z., Luo, L., Shao, C., Forner, J., Lohmann, J.U. et al. (2020) WUSCHEL triggers innate antiviral immunity in plant stem cells. *Science*, **370**, 227–231.
- Wu, J., Zhu, W. and Zhao, Q. (2022) Salicylic acid biosynthesis is not from phenylalanine in *Arabidopsis*. *J. Integr. Plant Biol.* **65**, 881–887.
- Xu, X., Crow, M., Rice, B.R., Li, F., Harris, B., Liu, L., Demesa-Arevalo, E. et al. (2021) Single-cell RNA sequencing of developing maize ears facilitates functional analysis and trait candidate gene discovery. *Dev. Cell*, **56**, 557–568.e556.
- Yadav, V., Wang, Z., Wei, C., Amo, A., Ahmed, B., Yang, X. and Zhang, X. (2020) Phenylpropanoid pathway engineering: an emerging approach towards plant defense. *Pathogens*, **9**, 312.
- Ye, J., Zhong, T., Zhang, D., Ma, C., Wang, L., Yao, L., Zhang, Q. et al. (2019) The auxin-regulated protein *ZmAuxRP1* coordinates the balance between root growth and stalk rot disease resistance in maize. *Mol. Plant*, **12**, 360–373.
- Zhang, Y. and Li, X. (2019) Salicylic acid: biosynthesis, perception, and contributions to plant immunity. *Curr. Opin. Plant Biol.* **50**, 29–36.
- Zhang, Y., He, J., Jia, L.J., Yuan, T.L., Zhang, D., Guo, Y., Wang, Y. et al. (2016) Cellular tracking and gene profiling of *Fusarium graminearum* during maize stalk rot disease development elucidates its strategies in confronting phosphorus limitation in the host apoplast. *PLoS Pathog.* **12**, e1005485.
- Zhang, T.Q., Xu, Z.G., Shang, G.D. and Wang, J.W. (2019) A single-cell RNA sequencing profiles the developmental landscape of *Arabidopsis* root. *Mol. Plant*, **12**, 648–660.
- Zhang, T.Q., Chen, Y., Liu, Y., Lin, W.H. and Wang, J.W. (2021a) Single-cell transcriptome atlas and chromatin accessibility landscape reveal differentiation trajectories in the rice root. *Nat. Commun.* **12**, 2053.
- Zhang, T.Q., Chen, Y. and Wang, J.W. (2021b) A single-cell analysis of the *Arabidopsis* vegetative shoot apex. *Dev. Cell*, **56**, 1056–1074.e1058.
- Zhao, C., Johnson, B.J., Kositsup, B. and Beers, E.P. (2000) Exploiting secondary growth in *Arabidopsis*. Construction of xylem and bark cDNA libraries and cloning of three xylem endopeptidases. *Plant Physiol.* **123**, 1185–1196.
- Zhu, M., Chen, Y., Ding, X.S., Webb, S.L., Zhou, T., Nelson, R.S. and Fan, Z. (2014) Maize Elongin C interacts with the viral genome-linked protein, VPG, of Sugarcane mosaic virus and facilitates virus infection. *New Phytol.* **203**, 1291–1304.

Supporting information

Additional supporting information may be found online in the Supporting Information section at the end of the article.

Figure S1 The artificial inoculation establishment of *Fusarium verticillioides* (*Fv*) infection in maize seedling roots.

Figure S2 scRNA-seq data quality evaluation, GO enrichment, and gene expression in seven cell types between Qi319 and B104.

Figure S3 RNA *in situ* hybridization analysis of cell type-specific marker genes.

Figure S4 Differential expression profiles of DEGs between *Fv*-infected and mock-inoculated conditions in seven cell types of Qi319 and B104 seedling root tips.

Figure S5 Expression heatmaps of marker and reported resistance genes in seven cell types of B104 and Qi319, KEGG pathways of *Fv*-responsive genes, and overlapped genes among DEGs in scRNA-seq data and predicted genes from previously published QTLs and QTNs.

Figure S6 Expression profiles of 12 maize known resistance-related genes post *Fv* infection.

Figure S7 Vector construction, maize transformant, and gene expression analysis to investigate functions of *ZmWOX5b* and *ZmPIN1a* genes.

Figure S8 Expression levels of maize disease resistance related genes in *ZmWOX5b* and *ZmPIN1a* transgenic plants post *Fv* infection.

Appendix S1 Supplemental methods.

Appendix S2 Details of abbreviations of Figure 7.

Table S1 Summary of scRNA-seq data in maize root tips.

Table S2 The list of 1950 marker genes in 21 cell clusters.

Table S3 856 independent marker genes of seven cell types in this study and other studies.

Table S4 Significant KEGG pathways for DEGs between cell cluster 13 and cell cluster 18.

Table S5 32 maize disease resistance related genes used in this study.

Table S6 Differentially expressed genes enriched in resistance-related biological process (yellow color) in seven cell types of B104 and Qi319.

Table S7 14 significant modules and 3596 genes identified by weighted gene co-expression network analysis.

Table S8 The category of 86 overlapped genes predicted by published QTLs or QTNs and distributed in *Fv*-responsive co-expression modules.

Table S9 148 key regulators and their predicted target genes in *Fv*-responsive co-expression modules identified by GENIE3.

Table S10 16 known maize resistance genes and 42 QTL-/QTN-associated *Fv* resistance related genes that are used for immunity network construction.

Table S11 Probes used for RNA *in situ* hybridization.

Table S12 The primers used in this study.